



University of Dundee

### **Exploiting the 2-Amino-1,3,4-thiadiazole Scaffold To Inhibit Trypanosoma brucei Pteridine Reductase in Support of Early-Stage Drug Discovery**

Linciano, Pasquale; Dawson, Alice; Pöhner, Ina; Costa, David M.; Sá, Monica S.; Cordeiro Da Silva, Anabela; Luciani, Rosaria; Gul, Sheraz; Witt, Gesa; Ellinger, Bernhard; Kuzikov, Maria; Gribbon, Philip; Reinshagen, Jeanette; Wolf, Markus; Behrens, Birte; Hannaert, Véronique; Michels, Paul A. M. ; Nerini, Erika; Pozzi, Cecilia; di Pisa, Flavio; Landi, Giacomo; Santarem, Nuno; Ferrari, Stefania; Saxena, Puneet; Lazzari, Sandra; Cannazza, Giuseppe; Freitas-Junior, Lucio H.; Moraes, Carolina B.; Pascoalino, Bruno S.; Alcântara, Laura M.; Bertolacini, Claudia P.; Fontana, Vanessa; Wittig, Ulrike; Müller, Wolfgang; Wade, Rebecca C.; Hunter, William N.; Mangani, Stefano; Costantino, Luca; Costi, Maria P.

*Published in:*  
ACS Omega

*DOI:*  
[10.1021/acsomega.7b00473](https://doi.org/10.1021/acsomega.7b00473)

*Publication date:*  
2017

*Document Version*  
Publisher's PDF, also known as Version of record

[Link to publication in Discovery Research Portal](#)

*Citation for published version (APA):*

Linciano, P., Dawson, A., Pöhner, I., Costa, D. M., Sá, M. S., Cordeiro Da Silva, A., ... Costi, M. P. (2017). Exploiting the 2-Amino-1,3,4-thiadiazole Scaffold To Inhibit Trypanosoma brucei Pteridine Reductase in Support of Early-Stage Drug Discovery. ACS Omega, 2(9), 5666-5683. DOI: 10.1021/acsomega.7b00473

# Exploiting the 2-Amino-1,3,4-thiadiazole Scaffold To Inhibit *Trypanosoma brucei* Pteridine Reductase in Support of Early-Stage Drug Discovery

Pasquale Linciano,<sup>†</sup> Alice Dawson,<sup>‡</sup> Ina Pöhner,<sup>∇</sup> David M. Costa,<sup>§</sup> Monica S. Sá,<sup>§</sup> Anabela Cordeiro-da-Silva,<sup>§,||</sup> Rosaria Luciani,<sup>†</sup> Sheraz Gul,<sup>⊥</sup> Gesa Witt,<sup>⊥</sup> Bernhard Ellinger,<sup>⊥</sup> Maria Kuzikov,<sup>⊥</sup> Philip Gribbon,<sup>⊥</sup> Jeanette Reinshagen,<sup>⊥</sup> Markus Wolf,<sup>⊥</sup> Birte Behrens,<sup>⊥</sup> Véronique Hannaert,<sup>#</sup> Paul A. M. Michels,<sup>#,|||</sup> Erika Nerini,<sup>†,§§</sup> Cecilia Pozzi,<sup>¶</sup> Flavio di Pisa,<sup>¶</sup> Giacomo Landi,<sup>¶</sup> Nuno Santarem,<sup>§</sup> Stefania Ferrari,<sup>†</sup> Puneet Saxena,<sup>†,⊥⊥</sup> Sandra Lazzari,<sup>†</sup> Giuseppe Cannazza,<sup>†</sup> Lucio H. Freitas-Junior,<sup>††,###</sup> Carolina B. Moraes,<sup>††</sup> Bruno S. Pascoalino,<sup>††</sup> Laura M. Alcântara,<sup>††</sup> Claudia P. Bertolacini,<sup>††</sup> Vanessa Fontana,<sup>††</sup> Ulrike Wittig,<sup>‡‡</sup> Wolfgang Müller,<sup>‡‡</sup> Rebecca C. Wade,<sup>∇,○,◆</sup> William N. Hunter,<sup>\*,‡</sup> Stefano Mangani,<sup>\*,¶</sup> Luca Costantino,<sup>\*,†</sup> and Maria P. Costi<sup>\*,†,¶</sup>

<sup>†</sup>Dipartimento di Scienze della Vita, Università degli Studi di Modena e Reggio Emilia, Via Campi 103, 41125 Modena, Italy

<sup>‡</sup>Biological Chemistry & Drug Discovery, School of Life Sciences, The Wellcome Trust Building, University of Dundee, Dow Street, Dundee DD1 5EH, U.K.

<sup>§</sup>Instituto de Investigação e Inovação em Saúde, Instituto de Biologia Molecular e Celular, and <sup>||</sup>Departamento de Ciências Biológicas, Universidade do Porto, Rua Alfredo Allen 208, 4200-135 Porto, Portugal

<sup>⊥</sup>Fraunhofer-IME SP, Schnackenburgallee 114, D-22525 Hamburg, Germany

<sup>#</sup>Research Unit for Tropical Diseases, de Duve Institute and Laboratory of Biochemistry, Université catholique de Louvain, Avenue Hippocrate 74, B-1200 Brussels, Belgium

<sup>¶</sup>University of Siena, Via Aldo Moro 2, 53100 Siena, Italy

<sup>∇</sup>Molecular and Cellular Modeling Group and <sup>‡‡</sup>Scientific Databases and Visualization (SDBV) Group, Heidelberg Institute for Theoretical Studies, Schloss-Wolfsbrunnengasse 35, D-69118 Heidelberg, Germany

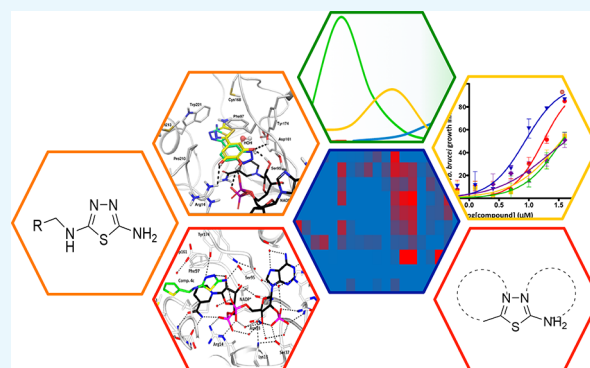
<sup>○</sup>Center for Molecular Biology (ZMBH), DKFZ–ZMBH Alliance, Heidelberg University, Im Neuenheimer Feld 282, D-69120 Heidelberg, Germany

<sup>◆</sup>Interdisciplinary Center for Scientific Computing (IWR), Heidelberg University, Im Neuenheimer Feld 205, D-69120 Heidelberg, Germany

<sup>††</sup>Laboratório Nacional de Biotecnologia CNPEM, Centro Nacional de Pesquisa em Energia e Materiais, Rua Giuseppe Máximo Scolfaro, 10.000, CEP 13083-970 Campinas/SP, Brasil

## Supporting Information

**ABSTRACT:** Pteridine reductase-1 (PTR1) is a promising drug target for the treatment of trypanosomiasis. We investigated the potential of a previously identified class of thiadiazole inhibitors of *Leishmania major* PTR1 for activity against *Trypanosoma brucei* (*Tb*). We solved crystal structures of several *Tb*PTR1-inhibitor complexes to guide the structure-based design of new thiadiazole derivatives. Subsequent synthesis and enzyme- and cell-based assays confirm new, mid-micromolar inhibitors of *Tb*PTR1 with low toxicity. In particular, compound **4m**, a biphenyl-thiadiazole-2,5-diamine with  $IC_{50} = 16 \mu M$ , was able to potentiate the antitrypanosomal activity of the dihydrofolate reductase inhibitor methotrexate (MTX) with a 4.1-fold decrease of the  $EC_{50}$  value. In addition, the antiparasitic activity of the combination of **4m** and MTX was reversed by addition of folic acid. By adopting an efficient hit discovery platform, we demonstrate, using the 2-amino-1,3,4-thiadiazole scaffold, how a promising tool for the development of anti-*T. brucei* agents can be obtained.



## INTRODUCTION

According to the World Health Organization (WHO), neglected tropical diseases afflict over 1 billion people.<sup>1</sup> Among them, parasitic infections caused by trypanosomatids represent a major challenge. Kinetoplastea is a class of flagellated parasitic protists, which includes various human pathogens transmitted by insect

vectors. Diseases that result from kinetoplastid infections include human African trypanosomiasis (HAT; also known as African

Received: April 18, 2017

Accepted: August 11, 2017

Published: September 11, 2017

sleeping sickness), which is caused by *Trypanosoma brucei gambiense* and *T. brucei rhodesiense*, Chagas disease caused by *Trypanosoma cruzi*, and various forms of leishmaniasis caused due to infection with different species of *Leishmania*.<sup>2</sup> Sleeping sickness is found across sub-Saharan Africa and evolves in two phases. The parasite first reaches the bloodstream and the lymphatic system, where it multiplies. At a later stage, the parasite crosses the blood–brain barrier, reaching the central nervous system and leading to death if untreated.<sup>3</sup> Therefore, therapies should be able to cure at least one of the two stages or both. Pentamidine and suramin are first choice drugs for the treatment of HAT. These drugs are specific for the first stage of pathology but they are completely ineffective in the second neuronal stage. Eflornithine, either in monotherapy or in combination with nifurtimox, is approved for second-stage treatment of HAT caused by *T. b. gambiense*.<sup>4</sup> For the latter stage, melarsoprol is also still used despite its high toxicity.<sup>5</sup> However, all of the drugs mentioned above have problems relating to poor efficacy, difficulties in administration, and side effects. In addition, drug resistance is also emerging. Thus, there is an urgent need to discover new improved and affordable drugs.<sup>3</sup> A target-based drug-discovery approach is a promising strategy for the discovery of new treatments for neglected diseases<sup>6</sup> and has been successfully exploited for the development of eflornithine (an inhibitor of ornithine decarboxylase).<sup>7</sup> Other targets, such as *N*-myristoyltransferase,<sup>8</sup> farnesyl transferase,<sup>9</sup> trypanothione reductase,<sup>10</sup> and cathepsin L,<sup>11</sup> have been validated in *T. brucei* (*Tb*), but no drugs acting on these targets have yet been approved for the treatment of HAT. One approach, successfully used in the treatment of some bacterial infections<sup>12</sup> and malaria,<sup>13</sup> could entail the use of drugs that target enzymes involved in folate metabolism. Targeting dihydrofolate reductase (DHFR) alone does not allow for successful antitrypanosomatid therapy because of the presence of pteridine reductase-1 (PTR1). PTR1 is a reduced nicotinamide adenine dinucleotide phosphate (NADPH)-dependent short-chain dehydrogenase/reductase (SDR) mainly involved in the reduction of conjugated and unconjugated pterins, such as biopterin.<sup>14,15</sup> PTR1 is responsible for the production of 10% of tetrahydrofolate required by the cell, and its expression is increased when parasite DHFR is inhibited by antifolate drugs. PTR1 thus provides the reduced folate necessary for parasite survival, thereby contributing to treatment failure.<sup>16,17</sup> PTR1 knockdown studies performed by RNA interference methodologies on blood stream form *T. brucei* compromised parasitic growth in vitro and in an animal host.<sup>17,18</sup> This evidence supports the importance of PTR1 for parasitic survival and indicates that it is a promising drug target for the treatment of HAT. However, *Tb*PTR1 inhibitors developed to date have limited antiparasitic activity against *T. brucei*.<sup>6,15,19–23</sup> In our previous work, we have identified thiadiazole derivatives as a new class of *Leishmania major* PTR1 (*Lm*PTR1) inhibitors that showed synergistic activity in combination with pyrimethamine (a DHFR inhibitor) against both *L. major* and *Leishmania mexicana* promastigotes.<sup>24,25</sup> The same behavior was observed with another PTR1 inhibitor class, namely pteridines, tested against the same *Leishmania* species. Thus, the emerging concept was that the selective PTR1 inhibitor alone did not show antiparasitic activity, and only the combination with a DHFR inhibitor, such as pyrimethamine, allowed the antiparasitic activity detection.<sup>26</sup> In the present work, we sought to exploit the thiadiazole scaffold as a source of new inhibitors of *Tb*PTR1, thereby targeting the folate/biopterin pathway with potential for activity against the parasite in

combination with DHFR inhibitors. Therefore, we focused mainly on compounds that showed PTR1 inhibition and no/low antiparasitic activity to exploit the above combination concept.

We have established an efficient hit discovery platform, which has a sound foundation in drug discovery that made use of a combination of computational design, organic synthesis, X-ray crystallography, enzyme inhibition, and antiparasitic activity assays as well as early-toxicity studies. The chemical starting points of the present study originated from a screen of the previously tested thiadiazole library<sup>24</sup> against *Tb*PTR1 and the *T. brucei* parasite. We then determined five ternary crystal structures of *Tb*PTR1 in complex with the cofactor NADP<sup>+</sup> and thiadiazole compounds, providing crucial data to support the design of improved inhibitors. Four new compound series, including a total of 57 compounds based on the 2-amino-1,3,4-thiadiazole scaffold, were designed, synthesized, and evaluated against *Tb*PTR1. In addition, structure–activity relationships (SAR) for *Tb*PTR1 were derived from comparison of computational docking results and crystallographic analyses. Initial toxicity assessments were carried out with a panel of five assays in high throughput screening (HTS) format. All compounds were evaluated for in vitro antiparasitic activity by phenotypic HTS against *T. brucei*. Finally, the most potent *Tb*PTR1 inhibitors were assayed in combination with the known DHFR inhibitor methotrexate (MTX) to evaluate the efficacy of the simultaneous inhibition of DHFR and PTR1 on *T. brucei* parasite growth.

## RESULTS AND DISCUSSION

**Selection of Compounds I–IV and X-ray Crystallographic Analyses.** Compounds I–X (Table S1) of the original thiadiazole library were selected for testing against *Tb*PTR1, based on molecular diversity and compound availability.<sup>24,27</sup> Only compounds II–IV showed measurable inhibition constants ( $K_i$ ) against *Tb*PTR1 in the range of 48–88  $\mu\text{M}$  (II  $K_i$  48  $\mu\text{M}$ ; III  $K_i$  53  $\mu\text{M}$ ; and IV  $K_i$  88  $\mu\text{M}$ ), thus behaving as weak *Tb*PTR1 inhibitors (Figure 1 and Table S1). Compound I showed an  $\text{EC}_{50}$  value of 35  $\mu\text{M}$  in the *T. brucei* parasite growth inhibition assay and no detectable inhibition of *Tb*PTR1 at 100  $\mu\text{M}$ . We could not detect antiparasitic activity for compounds II and III at concentrations up to 50  $\mu\text{M}$ . Compound IV was the only compound with low PTR1 inhibition and parasite growth inhibition (*Tb*PTR1  $K_i$  88  $\mu\text{M}$  and *T. brucei*  $\text{EC}_{50}$  170  $\mu\text{M}$ ). Compounds V–X showed low inhibition of *Tb*PTR1 (Table S1) at the tested concentration and no detectable growth inhibition of the *T. brucei* parasite at the concentration tested (50 or 100  $\mu\text{M}$ ). Compounds I–IV showed high toxicity against mammalian cells with selectivity indices ( $\text{EC}_{50}$  mammalian/ $\text{EC}_{50}$  *T. brucei*) lower than 1 (Table S1).

We carried out crystallographic analyses of *Tb*PTR1-inhibitor complexes to identify possible templates for medicinal chemistry exploration. Previous docking studies<sup>19</sup> indicated that the thiadiazole ring would form a stacking interaction between the nicotinamide ring of NADP<sup>+</sup> and Phe113 of *Lm*PTR1 (corresponding to Phe97 of *Tb*PTR1) and that lack of a cofactor results in a disordered binding pocket.<sup>28</sup> I–X were used for crystallization trials with *Tb*PTR1, and for four compounds I–IV (Figure 1) ternary complex structures [PDB ID: 2YHI (I); 2YHU (II); 4WCF (III); and 4WCD (IV)] were determined at high resolution (1.80, 2.01, 1.68, and 1.93 Å, respectively). Crystallographic statistics are presented in Table S2 in the Supporting Information.

The crystal structures are isomorphous with an asymmetric unit consisting of a homotetramer, the functional unit of

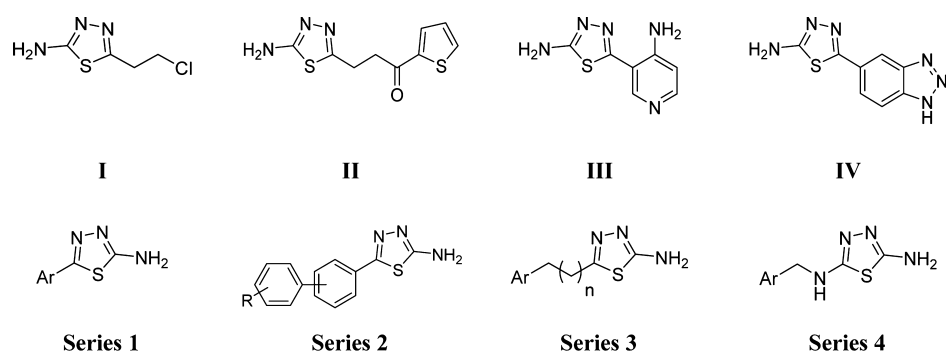


**Figure 1.** Chemical structures of previously synthesized thiazadiazoles (I–IV) crystallized with *Tb*PTR1–NADP<sup>+</sup> and the newly designed thiazadiazoles (series 1–4).

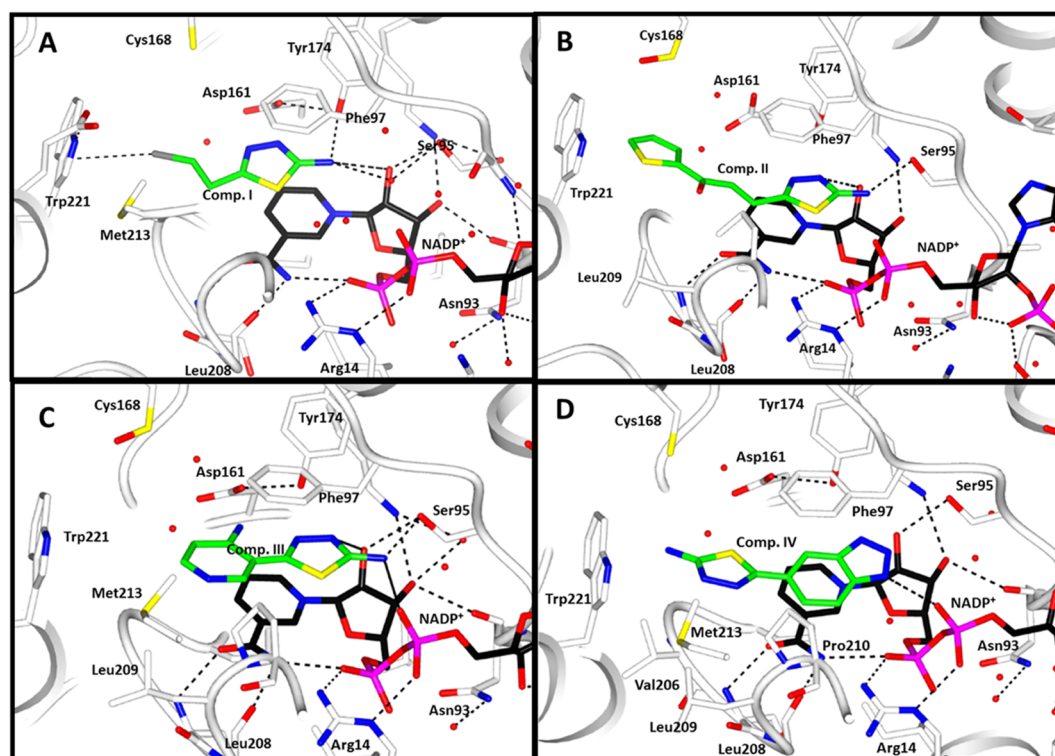


**Figure 2.** Noncovalent interactions involving thiazadiazole derivatives (stick representation, green carbons) in the *Tb*PTR1 active site: (A) compound I, (B) compound II, (C) compound III, and (D) compound IV. The thiazadiazole ring in all compounds (except IV) is sandwiched between the nicotinamide ring of cofactor NADP<sup>+</sup> (black carbons) and the phenyl ring of Phe97. H-bond interactions are represented by black dashed lines; water molecules are shown as red spheres. Model atoms except for carbons are color coded; protein carbons are white, oxygen red, sulfur yellow, chlorine gray, and phosphorous magenta. The protein backbone is drawn as a white cartoon. Note S-oxycysteine 168 (CSX) in (B,C). Interaction distances are reported in Table S2.1 in the [Supporting Information](#).

*Tb*PTR1. Each subunit has the typical structure of the short-chain SDR superfamily: a single  $\alpha/\beta$ -domain constructed from a seven-stranded parallel  $\beta$ -sheet sandwiched between two sets of  $\alpha$ -helices. The active site is an L-shaped depression, formed primarily by one subunit and blocked at one end by a partner subunit. NADP<sup>+</sup> binds in an extended conformation to form the binary complex essential for substrate/ligand binding. Analyses of the complexes with I–IV shows that the interaction of compounds I–III is mainly driven by the thiazadiazole moiety, which is indeed sandwiched between the nicotinamide of NADP<sup>+</sup> and Phe97 (Figure 2A–C). However, for compound IV (Figure 2D), it is the bulkier benzotriazole substituent that stacks in this position, placing the thiazadiazole moiety to participate in an edge–face interaction with Trp221 on the

periphery of the active site. The crystal structure of *Tb*PTR1–NADP<sup>+</sup>–I shows that the chloro-ethyl moiety of the inhibitor establishes a halogen bond with the  $\pi$ -system of Trp221 and van der Waals interactions with Val206, Pro210, and Met213. The amino group is H-bonded to Tyr174 OH and to the nicotinamide ribose, whereas a water molecule mediates the interactions with the side chain of Ser95 and the cofactor phosphate (Figure 2A). Because of the increased bulk of II and III, these compounds are placed further toward the cofactor, and the amino group displaces the ordered water observed in the *Tb*PTR1–NADP<sup>+</sup>–I active site (Figure 2B,C). A H-bond is formed between Tyr174 and nitrogen at position 3 of the thiazadiazole ring of compound II (not shown). The same nitrogen is within the H-bonding distance of the ribose moiety of the

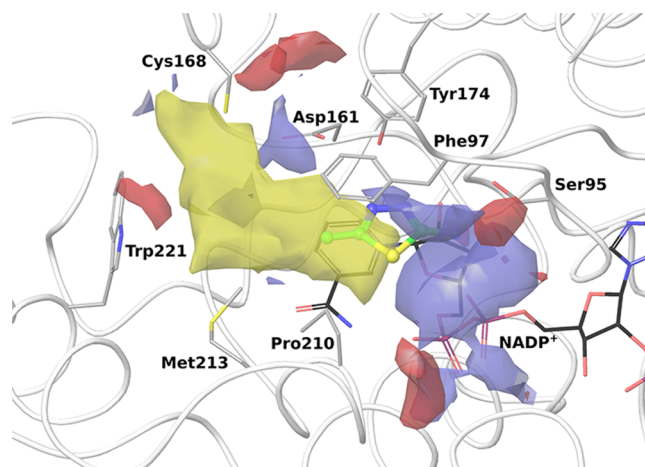
cofactor. This interaction is also visible in the complex with compound **III** (Figure 2C). Moreover, here the amino group on the aminopyridine ring is H-bonded to Asp161 and Tyr174 and participates in water-mediated interactions with the same aspartate and the carbonyl of Gly205 (not shown). Comparison between the binding modes of compounds **II–III** and folate (PDB: 3BMC; *Tb*PTR1–NADP<sup>+</sup>–folate complex) reveals that thiadiazole overlaps 2-amino-4-oxo pyrimidine of folic acid (see Figure S1 in Supporting Information). Notably, the amino group at position 2 of compounds **II** and **III** superimposes on the amino group in position 2 of the pteridine, forming similar H-bonds with the enzyme and the cofactor. In the case of **II**, the thiophene ring forms a T-shaped stacking interaction with Trp221 (Figure 2B). In the structure of the ternary complex *Tb*PTR1–NADP<sup>+</sup>–**IV** (Figure 2D), although similar to the other inhibitor complexes, one active site of the tetramer does not possess electron density for either the cofactor or the inhibitor. Moreover, in this subunit, the loop adjacent to the active site, including residues from 209 to 217, is disordered and hence excluded from our model. In addition to the different stacking arrangement described for compound **IV**, a series of polar interactions stabilize the benzotriazole position. The nitrogen at position 1 forms a H-bond with NADP<sup>+</sup> phosphate, and cofactor ribose hydroxyl is within the hydrogen bonding distance of the benzotriazole nitrogens at positions 2 and 3 that are further involved in weak interactions with the hydroxyl groups of Ser95 and Tyr174, respectively.

Despite the modest biological profile of compounds **I–IV** as *Tb*PTR1 inhibitors, we sought to explore the potential of this class of compounds as *Tb*PTR1 inhibitors and anti-*T. brucei* agents, guided by the structural binding mode of the thiadiazole scaffold within *Tb*PTR1 observed in the four resolved crystallographic complexes. The design of new thiadiazole derivatives focused on the optimization of the molecular interactions described herein, exploiting the most reliable binding mode of compounds **I–III**. In our design, we aimed at identifying a *Tb*PTR1 inhibitor that can show a synergistic effect in combination with a DHFR inhibitor; therefore, the antiparasitic activity of the thiadiazole derivative *per se* was not considered to be a requirement for the synergistic combination effect.

**Design of 2-Amino-1,3,4-thiadiazole Derivatives.** To initiate the design of new 2-amino-1,3,4-thiadiazole derivatives, molecular interaction fields were calculated (SiteMap<sup>27</sup>) to understand how the ligands complement the receptor and how extensions into adjacent regions could promote binding. The structures of *Tb*PTR1 with compounds **I–IV** show similar interaction fields in the active site. However, we opted to exploit for the development of the 2-amino-1,3,4-thiadiazole core, the binding mode of compounds **I–III**, as it is conserved in three of the four X-ray crystal structures, thus providing a reliable premise for the structure-based inhibitor design. These structures reveal a large hydrophobic region between Phe97 and the nicotinamide, extending toward the surface of the protein next to Trp221, which closes the *Tb*PTR1 active site (Figure 3). Two distinct hydrophilic regions were also identified, which can be further divided into regions favorable for H-bond donors and acceptors. One of these is located in the depth of the catalytic site, and the phosphate groups of the NADP<sup>+</sup> cofactor, Ser95 and Tyr174, delineate it. This region is split into a region favorable for H-bond donors, which is in part addressed by the amino group in position 2 on the main core scaffold, and a small favorable interaction site for H-bond acceptors. The second hydrophilic region is close to Asp161 and represents an additional favorable interaction site for

H-bond donors. Therefore, extending from the 2-amino-1,3,4-thiadiazole core, which establishes key interactions, we modified position 5 of the ring with substituents designed to interact with the residues lining the pocket of the binding site. Four series of compounds were synthesized (Figure 1). In the first two series, a phenyl or heteroaromatic ring (compounds **1a–t**, Chart 1) or a biphenyl system (compounds **2a–g**, Chart 2) was bound to the thiadiazole ring to fill the large hydrophobic region located next to the catalytic site. In the third series (compounds **3a–k**, Chart 3), the aromatic ring was spaced with a short aliphatic chain (one to three carbon atoms) to reach the position occupied by the *p*-amino-benzoic acid (PABA) ring of the natural folic acid substrate. The only exception is compound **3i**, which has the distal aromatic ring replaced by dimethylamine; it was commercially available and was purchased. Compound **II** (showing the lowest  $K_i$  value in the initial screen) was resynthesized as an internal reference (**3k**). Then, to closely match the nitrogen system of the pteridine moiety of the natural PTR1 substrate and to potentially address the additional region favorable for H-bond donors close to Asp161, a fourth series of thiadiazoles was designed (compounds **4a–s**, Chart 4), introducing nitrogen in position 5 of the thiadiazole ring.

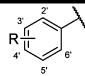
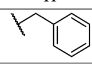
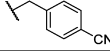
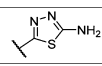
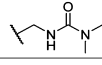
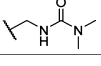
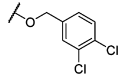
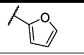
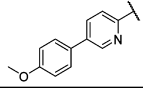
**Chemistry.** Four series of thiadiazoles were synthesized: 5-aryl-2-amino-1,3,4-thiadiazoles (**1a–t**); 5-biphenyl-2-amino-1,3,4-thiadiazoles (**2a–g**); 5-alkyl-2-amino-1,3,4-thiadiazoles (**3a–k**), and 2,5-diamino-1,3,4-thiadiazoles (**4a–s**). For the synthesis of compounds **1a–t**, **2a–g**, and **3a–k**, the closure of



**Figure 3.** Energetically favorable interaction sites in the *Tb*PTR1 binding site computed using SiteMap for the crystal structure with compound **III** (4WCF). Favorable regions for hydrophobic groups are shown by yellow isocontours (at  $-0.5$  kcal/mol); for hydrogen bond donors and acceptors, they are shown by isocontours (at  $-8$  kcal/mol) in blue and red, respectively. NADP<sup>+</sup> (in black) and some important residues delineating the pocket (in white) are shown in stick representation. The 2-amino-1,3,4-thiadiazole moiety (in ball and stick, green carbons) of compound **III** is displayed for reference.

the thiadiazole ring was optimized and four synthetic pathways were developed (Scheme 1). The choice of the synthetic method was constrained by the compatibility between the sensitive chemical functions present in the molecule and the strong oxidizing and dehydrating agents necessary for the thiadiazole ring closure. Method A, depicted in Scheme 1, requires the condensation of the appropriate alkyl/aryl carboxylic acid with thiosemicarbazide in the presence of phosphorus(V)-oxachloride (POCl<sub>3</sub>).<sup>29</sup> Compounds **1i**, **1j–k**, **1o**, **2b**, **3a**, **3c–d**, and **3f–g**

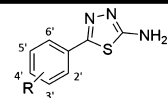
Chart 1. 2-Amino-1,3,4-thiadiazoles Containing a Substituted Aryl Moiety in Position 5<sup>a</sup>

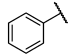
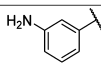
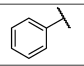
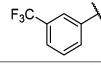
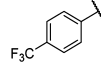
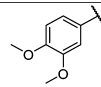
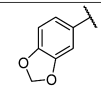
Entry							Synthetic Scheme	% Inhibition <i>Tb</i> PTR1 at 50 μM [IC <sub>50</sub> in μM]	% Inhibition <i>T. brucei</i> at 50 μM [EC <sub>50</sub> in μM] <sup>a</sup>
	R2'	R3'	R4'	R5'	R6'				
1a	H	H	H	H	H	1b	25.3±1.2	21.0	
1b	H	H	CH <sub>2</sub> NH <sub>2</sub>	H	H	1c	7.7±0.6	93.0 [0.8]	
1c	H	OCH <sub>3</sub>	OCH <sub>3</sub>	H	H	1d	9.4±0.3	64.3	
1d	H	OH	OH	H	H	3	16.7±1.0	78.6 [18.3]	
1e	H	OCH <sub>3</sub>	OCH <sub>3</sub>	OCH <sub>3</sub>	H	1d	13.5±0.4	1.4	
1f	H	OH	OH	OH	H	3	44.9±0.9 [41.0]	100.0 [1.0]	
1g	OCH <sub>3</sub>	H	H	H	OCH <sub>3</sub>	1d	14.1±1.2	4.2	
1h	OCH <sub>3</sub>	H	H	H	H	1d	24.1±1.0	NI	
1i	H	Br	H	H	H	1a	34.2±1.5	1.8	
1j	H	NH <sub>2</sub>	H	H	H	1a	27.0±0.4	1.0	
1k	H	NO <sub>2</sub>	H	H	H	1a	15.6±1.1	1.4	
1l	H	Cl	Cl	H	H	1d	15.6±0.7	30.0	
1m		H	H	H	H	1d	9.1±0.5	84.0 [47.0]	
1n		H	H	H	H	1d	25.6±0.7	43.9 [52.0]	
1o	NH <sub>2</sub>	H		H	H	1a	23.4±0.1	1.6	
1p	H	H		H	H	2	5.3±0.9	NI	
1q	H		H	H	H	2	2.5±0.2	1.2	
1r	H	H		H	H	1d	NI	58.4	
<b>Ar-</b>									
1s							1c	9.0±0.8	NI
1t							1d	8.3±1.8	28.9

<sup>a</sup>Standard deviation is within ±10% of the value. NI; no inhibition.

were synthesized following the described procedure. It was not possible to obtain the thiadiazoles **1a**, **3e**, **3h**, and **3j–k** in the presence of POCl<sub>3</sub>; for these compounds, the use of concentrated sulfuric acid as a dehydrating agent at room temperature overnight allowed the final compounds to be obtained in good yield (method B, Scheme 1).<sup>29</sup> The synthesis of thiadiazoles **1b**, **1t**, **3b**, and intermediate **6** required milder experimental conditions because several attempts with sulfuric acid or POCl<sub>3</sub> led to decomposition. Thus, the thiadiazole ring closure was in this case performed by condensation between alkyl/aryl nitrile **9a–d** and thiosemicarbazide in concentrated trifluoroacetic acid at 60 °C (method C, Scheme 1).<sup>29</sup> Thiadiazole **6** thus obtained was not isolated and was instead directly used in the next step without further purification. When it was not possible to use these strong oxidizing and dehydrating agents because of the presence of sensitive chemical functions, an alternative synthetic route that requires oxidation of aryl-thiosemicarbazone, prepared from the relative aldehydes, with an ethanolic solution of FeCl<sub>3</sub> at 60 °C was shown to be successful (method D, Scheme 1).<sup>29</sup> Ureido-thiadiazoles **1p–q** were prepared through a reaction of **1b** and **6**, respectively, with dimethylcarbonyl chloride in dry dichloromethane (DCM)

(Scheme 2). Because it was not possible to directly prepare catecholic thiadiazole with any of the experimental procedures described above, 3',4'-dihydroxy-phenyl-1,3,4-thiadiazole (**1d**) and 3',4',5'-trihydroxy-phenyl-1,3,4-thiadiazole (**1f**) were obtained through demethylation of the respective methoxylated thiadiazoles **1c** and **1e**, using boron tribromide (Scheme 3). Finally, compounds **4a–s** were all synthesized through aromatic nucleophilic substitution between the appropriate commercial alkylamine and 5-amino-2-bromo-1,3,4-thiadiazole (Scheme 4). Nitriles **9a** (benzylcyanide) and **9b** [4-(aminomethyl)benzonitrile] were commercially available and used as purchased. 3-(4-Methoxyphenyl)pyridin-2-carbonitrile (**9c**) was instead prepared as depicted in Scheme 5: 3-bromo-5-pyridin-carboxaldehyde was converted first to 3-bromo-5-pyridin-carbonitrile (**7**) with concentrated ammonia in tetrahydrofuran (THF) at room temperature, using iodine as the oxidant.<sup>30</sup> Then, **7** was reacted with 4-methoxyphenylboronic acid through the standard Suzuki reaction to obtain biphenyl nitrile **9c**.<sup>31</sup> Similarly, for the synthesis of 3-(aminomethyl)benzonitrile (**9d**), 3-(bromomethyl)benzonitrile was reacted with potassium phthalimide under standard S<sub>N</sub>2 conditions to give the corresponding phthalimide **8**. Phthalimide was then converted to amine with

Chart 2. 2-Amino-1,3,4-thiadiazoles Substituted with a Biphenyl System in Position 5<sup>a</sup>


Entry	R2'	R3'	R4'	R5'	R6'	Synthetic Scheme	% Inhibition <i>Tb</i> PTR1 at 50 $\mu$ M [IC <sub>50</sub> in $\mu$ M]	% Inhibition <i>T. brucei</i> at 50 $\mu$ M [EC <sub>50</sub> in $\mu$ M] <sup>a</sup>
2a	H	H		H	H	1d	10.8±0.4	43.1
2b	H	H		H	H	1a	16.2±0.5	33.4
2c	H		H	H	H	1d	25.2±1.4	14.4
2d	H		H	H	H	1d	4.6±1.0	94.8 [37.0]
2e	H		H	H	H	1d	6.6±0.6	92.1 [42.0]
2f	H		H	H	H	1d	8.6±0.6	9.5
2g	H		H	H	H	1d	4.0±0.4	10.4

<sup>a</sup>Standard deviation is within  $\pm 10\%$  of the value.

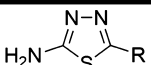
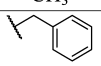
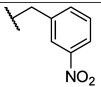
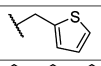
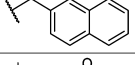
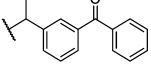
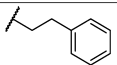
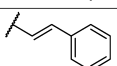
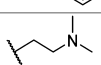
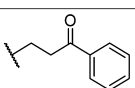
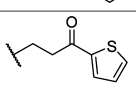
aqueous hydrazine to give the desired nitrile **9d** (Scheme 5). Finally, for the synthesis of thiosemicarbazones **11a–o**, aldehydes **10a–e** and **10i–j** were commercially available and used as purchased. Biphenylaldehydes **10k–o** were prepared using the Suzuki reaction between 3-bromobenzaldehyde and the appropriate phenylboronic acid. The same synthetic reaction was performed between 3-(bromomethyl)benzaldehyde and phenylboronic acid or 4-cyanophenylboronic acid to give benzylbenzaldehydes **10f** and **10g**, respectively. Aldehyde **10h** was instead prepared via S<sub>N</sub>2 reaction between *p*-hydroxybenzaldehyde and 3,4-dichlorobenzylchloride. Thus, aryl aldehydes **10a–o** were condensed with thiosemicarbazide to obtain the respective aryl-thiosemicarbazones (**11a–o**) (Scheme 6).

**PTR1 Inhibition Studies.** All 57 new thiadiazoles **1a–t**, **2a–g**, **3a–k**, and **4a–s** were evaluated for their inhibitory activity against *Tb*PTR1. Compounds displaying a percentage of inhibition against *Tb*PTR1 above 30% at 50  $\mu$ M were further analyzed in dose–response experiments between 0.001 and 100  $\mu$ M to enable the determination of their IC<sub>50</sub> values. The IC<sub>50</sub> value of pyrimethamine (IC<sub>50</sub> = 0.09  $\mu$ M against *Tb*PTR1), a DHFR inhibitor also able to inhibit PTR1, was measured routinely as a standard. The activity data of the entire panel of compounds are reported in Charts 1–4. The general activity profile of the studied compounds is shown in Figure 4. Among the 57 thiadiazoles synthesized, **1f**, **4c**, **4e–f**, **4h–i**, **4m–o**, and **4q** were associated with IC<sub>50</sub> values in the range of 16 to 112  $\mu$ M (Charts 1–4), resulting in a 2 to 12-fold improved inhibition effect toward *Tb*PTR1 in comparison to the initial screening hits **II–IV** (IC<sub>50</sub> > 200  $\mu$ M). With the exception of **1f** (*Tb*PTR1, IC<sub>50</sub> 41  $\mu$ M), the most active *Tb*PTR1 inhibitors belong to the 2,5-diamino-1,3,4-thiadiazoles (series 4) with the best compound **4m** showing an IC<sub>50</sub> of 16  $\mu$ M. *Tb*PTR1 and *Tb*DHFR use similar substrates such as dihydrofolic acid; thus, PTR1 inhibitors can also interact with DHFR. Therefore, to evaluate the potential

dual PTR1 and DHFR inhibition, all compounds were tested against *Tb*DHFR. However, none of the compounds showed any significant inhibitory activity against *Tb*DHFR (Table S3). The compounds that showed the best inhibitory activity against *Tb*PTR1 were selected for further studies.

**Crystallographic Studies of Compound 4c.** Cocrystallization trials were performed with ten thiadiazole compounds that showed the best inhibition against *Tb*PTR1 (**1f**, **4c**, **4e–f**, **4h–i**, **4m–o**, and **4q**). Only compound **4c**, belonging to the fourth series, resulted in a ternary complex at an acceptable resolution. **4c** is a comparatively modest inhibitor of *Tb*PTR1 showing an IC<sub>50</sub> of 112  $\mu$ M. The structure of the complex *Tb*PTR1–NADP<sup>+</sup>–**4c** was determined to 1.92 Å resolution (PDB ID: 5IZC). Statistics for the data collection and refinement are presented in Table S2 in the Supporting Information. Ligand placement in the active site and key interactions are depicted in Figure 5. **4c** adopts the same binding mode in all four subunits of the enzyme, only with differing orientations of the thiophene ring. The electron density for **4c** is best defined in subunits A and D. The **4c** thiadiazole ring binds in a  $\pi$ -sandwich between the nicotinamide of NADP<sup>+</sup> and Phe97, as previously described. The 2-amino group on the thiadiazole of **4c** is within the hydrogen bonding distance of both NADP<sup>+</sup> phosphate and Ser95 OH. The thiadiazole nitrogen in position 3 forms a bifurcated interaction with the NADP<sup>+</sup> ribose OH and Tyr174 OH. Furthermore, the thiadiazole nitrogen in position 4 is within the hydrogen bonding distance of Tyr174 OH. The thiophene moiety of **4c** lodges in the hydrophobic cavity defined by Cys168, Val206, Leu209, Met213, and Trp221. The above interactions are retained in all four subunits of the *Tb*PTR1 tetramer. Cys168 is chemically modified to S,S-(2-hydroxyethyl)thiocysteine (defined also as CME in Figure 5) because of the reaction with  $\beta$ -mercaptoethanol present in the purification buffer.

Chart 3. 2-Amino-1,3,4-thiadiazoles Substituted in Position 5 with an (Aryl-)aliphatic Chain<sup>a</sup>

Entry	R	Synthetic Scheme		
			% Inhibition <i>Tb</i> PTR1 at 50 $\mu$ M [IC <sub>50</sub> in $\mu$ M]	% Inhibition <i>T. brucei</i> at 50 $\mu$ M [EC <sub>50</sub> in $\mu$ M] <sup>a</sup>
3a	CH <sub>3</sub>	1a	5.4±0.7	NI
3b		1c	8.1±0.2	NI
3c		1a	15.8±0.5	0.8
3d		1a	18.5±0.6	7.5
3e		1b	20.9±0.3	0.4
3f		1a	47.2±0.4	88.0 [20.0]
3g		1a	7.6±0.3	NI
3h		1d	34.3±1.2	82.7 [58.0]
3i		Com	5.6±0.6	NI
3j		1b	12.9±0.7	1.2
3k		1b	26.0±0.7	60.7

<sup>a</sup>Standard deviation is within  $\pm 10\%$  of the value. NI; no inhibition.

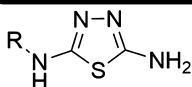
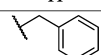
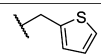
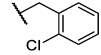
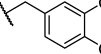
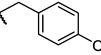
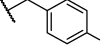
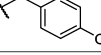
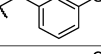
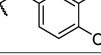
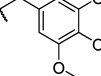
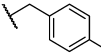
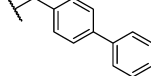
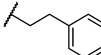
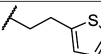
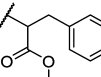
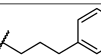
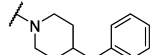
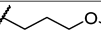
**SAR for *Tb*PTR1 Inhibition.** Although the design of the 57 compounds was largely based on the crystal structures available for compounds I–IV, the observed PTR1 inhibition potency did not reflect the expected effects of the structural modifications. This suggests that the binding mode observed in the crystal structures might be altered for the modified compounds. Therefore, to explore possible alternative binding modes, we docked all synthesized compounds in the *Tb*PTR1 binding site. Combining the predicted binding modes with the crystal structures enabled us to explain the SAR for the compounds' inhibitory potential against *Tb*PTR1. Common interactions, such as stacking of the thiadiazole core moiety between Phe97 and nicotinamide, were generally reproduced in docking. Because of the small size of the ligand core, rotation within the pocket did however result in different hydrogen bonding patterns, for example, involving the cofactor phosphate and ribose, Ser95, Asp161, and Tyr174, as indicated by differing arrangements of the thiadiazole core in Figure 6B–D.

A direct connection of the thiadiazole core with an aryl moiety, as in series 1 (Chart 1: 5-aryl-1,3,4-thiadiazoles), may lead to a competition for the stacking position in the *Tb*PTR1 binding site, which pushes the core moiety closer to the cofactor to introduce unfavorable contacts, as observed in almost all docked complexes of these compounds. Series 1 compounds consistently show low *Tb*PTR1 inhibition. Only compound 1f, bearing a pyrogallol substituent, presents a moderate IC<sub>50</sub> value of 41  $\mu$ M. We hypothesize that the pyrogallol moiety occupies the

stacking position and forms several H-bonds with Tyr174 and cofactor phosphates and ribose (Figure 6A). Because this alternative binding mode is specific for 1f, it may explain the observed activity. Series 2 and series 3 compounds only yielded <47% inhibition of *Tb*PTR1 at 50  $\mu$ M. In series 2 (Chart 2: 5-biphenyl-1,3,4-thiadiazoles), the elongated conformation of the compounds fits the binding pocket poorly, whereas in series 3 (Chart 3: 5-aryl-aliphatic-1,3,4-thiadiazoles), the long, flexible aliphatic linkers tend to be disfavored and are often placed in a polar and thus unfavorable environment, further leading to an unfavorable placement of substituents. Series 4 (Chart 4: 2,5-diamino-1,3,4-thiadiazoles) includes nine out of the nineteen compounds that yielded >30% inhibition of *Tb*PTR1 at 50  $\mu$ M, resulting in IC<sub>50</sub> values in the range of 16–112  $\mu$ M. Compounds of this class typically have a linker of 2–3 atoms between thiadiazole and further aryl substituents, including nitrogen in position 5. The second amino-nitrogen thereby allows for further favorable interactions, for example, with the carbonyl group of the cofactor, Asp161, or Tyr174, as indicated by the bound orientation of compound 4c in the crystal structure 5IZC (see Figure 5). Hence, series 4 allows the exploitation of the additional region favorable for H-bond donors, as identified by the SiteMap calculations (see also Figure 3). Although comparatively small compounds, such as 4i, show similar binding modes to that observed in the crystallographic complex of 4c (compare Figure S2A), larger compounds are locked in a binding orientation closely resembling that of folic acid, as shown in



Chart 4. 2,5-Diamino-1,3,4-thiadiazoles Containing Variations on the N<sup>5</sup>-Linked Group<sup>a</sup>

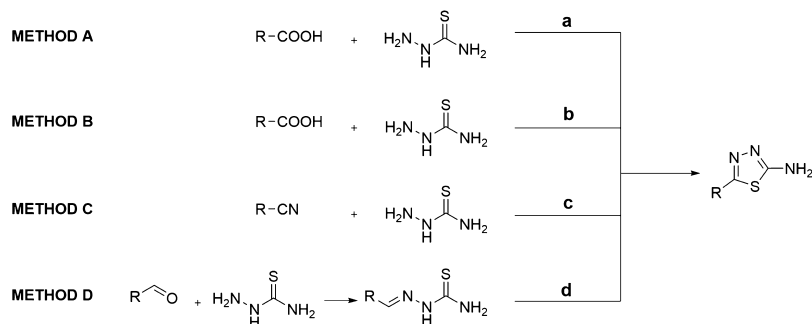
Entry	R	Synthetic Scheme		
			% Inhibition <i>Tb</i> PTR1 at 50 μM [IC <sub>50</sub> in μM]	% Inhibition <i>T. brucei</i> at 50 μM [EC <sub>50</sub> in μM] <sup>a</sup>
4a	H	4	14.2±0.8	NI
4b		4	39.5±0.9	NI
4c		4	50.6±2.6 [112.0]	NI
4d		4	21.8±2.2	NI
4e		4	48.5±2.1 [31.0]	NI
4f		4	37.7±0.5 [48.0]	NI
4g		4	14.7±1.7	33.0
4h		4	34.6±3.0 [70.0]	NI
4i		4	31.0±1.3 [56.0]	95.6 [16.0]
4j		4	8.4±1.2	45.1
4k		4	NI	NI
4l		4	18.6±0.8	10.8
4m		4	73.0±1.1 [16.0]	6.6
4n		4	36.7±2.0 [62.0]	4.0
4o		4	79.8±0.4 [25.0]	37.9
4p		4	3.9±0.3	0.4
4q		4	30.0±1.9 [57.0]	NI
4r		4	8.4±0.3	1.8
4s		4	11.8±0.3	NI

<sup>a</sup>Standard deviation is within ±10% of the value. NI; no inhibition.

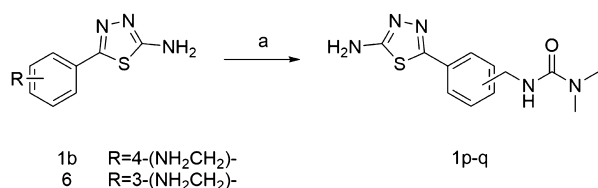
Figure 6B–D. A substrate-like complex thereby seems to correlate with enhanced activity because the docking mode of the majority of actives in this class best matches the folic acid orientation.

Compound **4m** has a linked biphenyl system and is the most active compound (*Tb*PTR1 IC<sub>50</sub> 16 μM). The thiadiazole position is stabilized by hydrogen bonding interactions with the cofactor and Ser95, and the phenyl ring systems of **4m** interact by π–π interactions and hydrophobic contacts with Phe97, Met163,

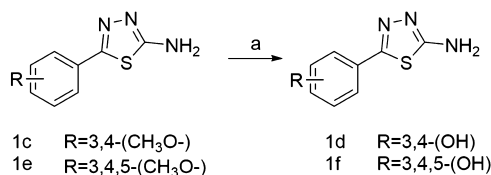
Phe171, Tyr174, Met213, and Trp221. Notably, as shown in Figure 6B, the biphenyl system adopts a substrate-like orientation, with the first phenyl ring mimicking the PABA moiety of folic acid and the second phenyl locking the compound in that orientation by spatial restraints. Similar observations can be made for compounds **4o** (*Tb*PTR1, IC<sub>50</sub> 25 μM) and **4e** (*Tb*PTR1, IC<sub>50</sub> 31 μM). Interestingly, **4n** (*Tb*PTR1, IC<sub>50</sub> 62 μM) shows an identical binding mode to **4o** but is about 3 times less active. In summary, compounds that are able to bind in a

Scheme 1. Synthetic Methods Employed for the Thiadiazole Ring Closure<sup>a</sup>

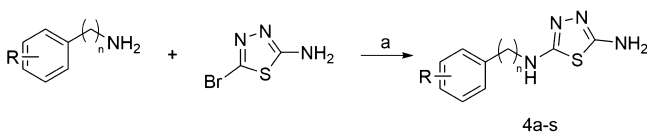
<sup>a</sup>(a) POCl<sub>3</sub>, neat, 80 °C, overnight; (b) H<sub>2</sub>SO<sub>4</sub> concn, neat, rt, overnight; (c) trifluoroacetic acid, neat, 60 °C, 6–12 h; and (d) FeCl<sub>3</sub> (2 equiv), EtOH aq 50%, 60 °C, 0.5–6 h.

Scheme 2. Synthesis of Dimethylcarbamyl Compounds 1p–q<sup>a</sup>

<sup>a</sup>Reagent and conditions: (a) dimethylcarbamyl chloride, DCM dry, N<sub>2</sub>, rt, 24 h.

Scheme 3. Synthesis of Hydroxylated Compounds 1d and 1f<sup>a</sup>

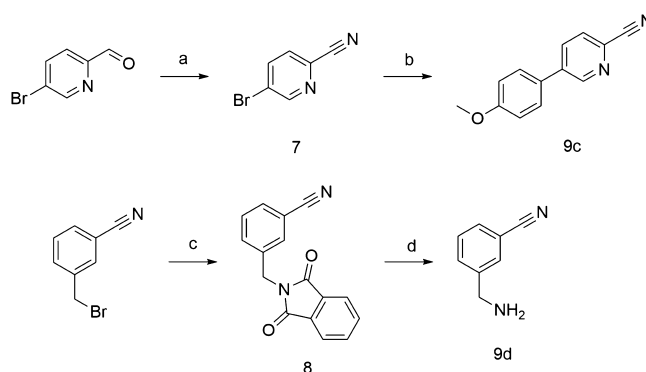
<sup>a</sup>Reagent and conditions: (a) BBr<sub>3</sub> 1.25 M in DCM, DCM dry, N<sub>2</sub>, 0 °C → rt, 1–3 h.

Scheme 4. Synthesis of 2,5-Diamino-1,3,4-thiadiazoles 4a–s<sup>a</sup>

<sup>a</sup>Reagent and conditions: (a) Triethylamine (2.5 equiv), THF, refl., 6 h.

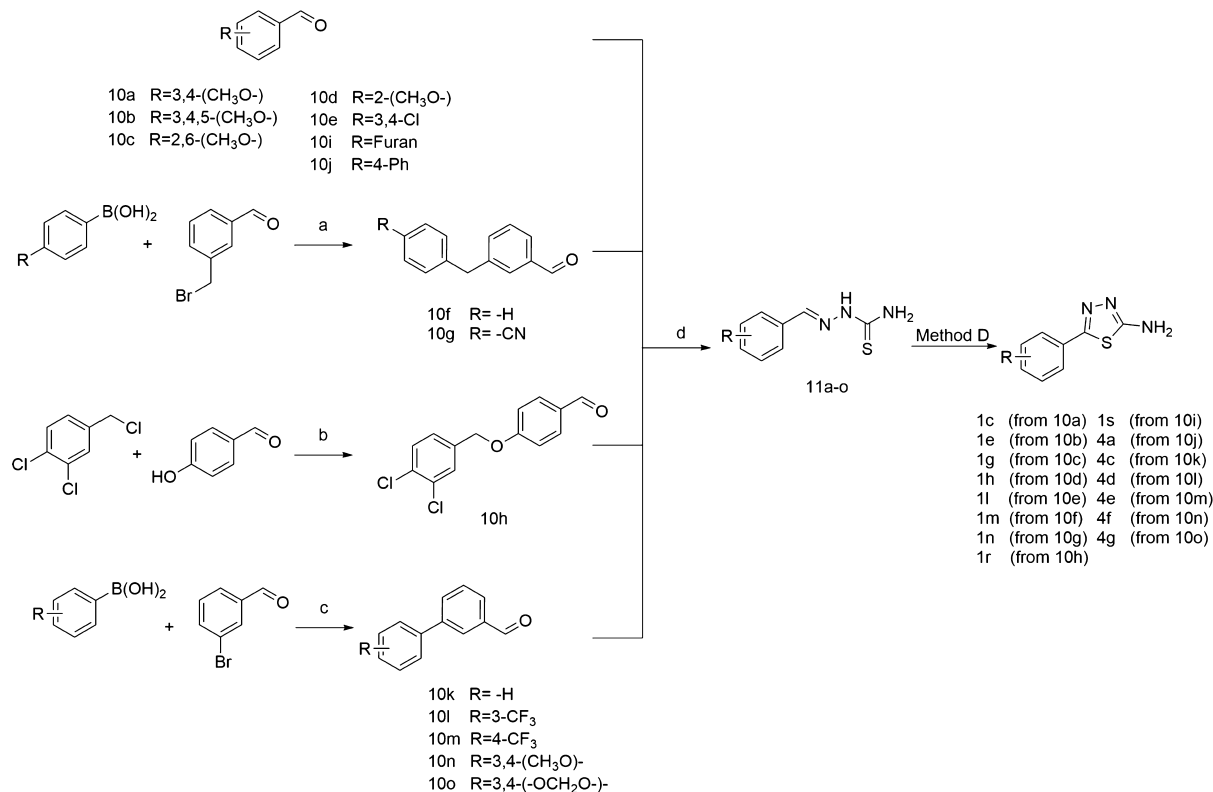
substrate-like orientation show the best *Tb*PTR1 inhibition profile. Despite the fact that direct correlation between the docking score and the % inhibition or IC<sub>50</sub> for the compounds could not be observed, we were able to deduce likely near native poses and describe a qualitative correlation between the observed binding mode in the crystallographic complexes, the docking results, and the anti-PTR1 activity of the compounds (“Docking Protocol Validation”, [Supporting Information](#)). Visual inspection of the interaction pattern and comparison with crystal structures were used to select the most likely poses, based on experimental evidence.

**Antiparasitic In Vitro Evaluation against Cultured *T. brucei*.** All compounds were evaluated for inhibitory activity on growth of in vitro cultured *T. b. brucei* through a HTS assay (a cell-based assay with a fluorescent readout) during a phenotypic

Scheme 5. Synthesis of Nitriles 9c–d<sup>a</sup>

<sup>a</sup>Reagent and conditions: (a) NH<sub>3</sub> aq 35%, I<sub>2</sub> (1.1 equiv), THF, rt, 1 h; (b) 4-methoxy-phenylboronic acid, Pd/C 10 mol %, Na<sub>2</sub>CO<sub>3</sub> aq 1 M, dioxane, 60 °C, 24 h; (c) potassium phthalimide, dimethylformamide (DMF), rt, 12 h; and (d) NH<sub>2</sub>NH<sub>2</sub> aq, THF, rt, 24 h.

screening campaign. The antiparasitic activity is expressed as the percentage of cell growth inhibition at 50 μM and is reported in [Charts 1–4](#). For the nine compounds (**1b**, **1d**, **1f**, **1m**, **1n**, **2d**, **3f**, **3h**, and **4i**) showing >75% inhibition, the EC<sub>50</sub> was also determined with results in the range of 0.8–58.0 μM. We observed no correlation between *Tb*PTR1 inhibition and antiparasitic activity ([Figure 7](#)). The data distribution in [Figure 7](#) highlights two distinct sets of compounds: cluster A includes all thiadiazoles that showed antiparasitic activity with EC<sub>50</sub> in the range of 0.8–58.0 μM (**1b**, **1d**, **1f**, **1m–n**, **2d–e**, **3f**, **3h**, and **4i**) but had poor efficacy against the target enzyme (<50% inhibition of *Tb*PTR1 at 50 μM) and is therefore likely to have a different target. On the other hand, cluster B comprises two compounds (**4m** and **4o**) that show the highest *Tb*PTR1 inhibition (IC<sub>50</sub> 16 and 25 μM, respectively) but poor antiparasitic activity when tested as single agents ([Figure 7](#), [Chart 4](#)). In addition, neither **4m** nor **4o** is able to inhibit parasitic *Tb*DHFR at 100 μM. We were able to identify better *T. brucei* growth inhibitors with respect to our starting compounds. In particular, compound **1b** showed 7.2-fold better activity with respect to compound **1** (EC<sub>50</sub> 0.8 μM and EC<sub>50</sub> 5.8 μM). All compounds were also evaluated for in vitro antiparasitic activity against the intracellular amastigote stage of *L. infantum*, but no compound showed antileishmanial activity >50% inhibition at 50 μM (Table S3, [Supporting Information](#)).<sup>32</sup> The best compounds with anti-*T. brucei* activity were **1b** and **1f**, but they did not show inhibition of *Tb*PTR1. Because of the lack of compounds exhibiting both *Tb*PTR1 inhibition and antiparasitic activity, our interest turned to the

Scheme 6. Synthesis of Aldehydes 10a–o and the Respective Thiosemicarbazones 11a–o<sup>a</sup>

<sup>a</sup>Reagents and conditions: (a) Pd/C 10 mol %, Na<sub>2</sub>CO<sub>3</sub> aq 1 M, dioxane, 60 °C, 24 h; (b) K<sub>2</sub>CO<sub>3</sub> (2.5 equiv), DMF, 120 °C, 2 h; (c) tetrakis 10 mol %, Na<sub>2</sub>CO<sub>3</sub> (2 equiv), water/dioxane 1:1, 60 °C, 6 h; and (d) FeCl<sub>3</sub> (2 equiv), EtOH aq 50%, 60 °C, 0.5–6 h.

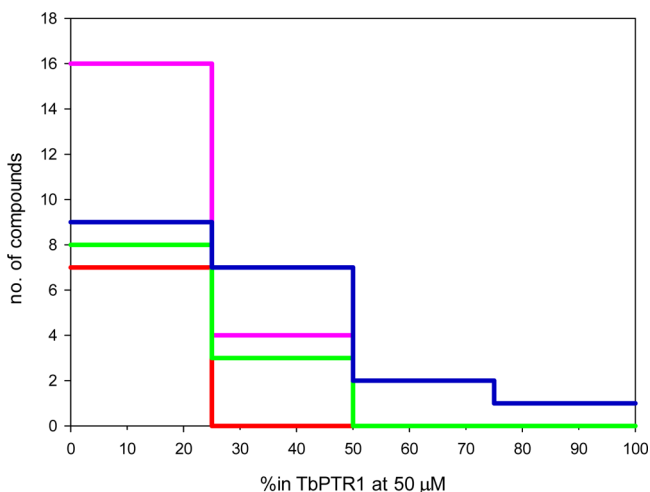


**Figure 4.** Activity profile against *T. b. brucei* (*y*-axis) observed for the newly synthesized thiadiazoles (**series 1**: purple line; **series 2**: red line; **series 3**: green line; and **series 4**: blue line) against the percentage of TbPTR1 inhibitory activity at 50 μM (*x*-axis).

evaluation of compounds **4m** and **4o** in combination with a TbDHFR inhibitor.

**Potentiating Effect of Thiadiazoles in Combination with MTX.** Given that inhibition of TbDHFR alone does not effectively kill the parasite because of a bypass via TbPTR1, a simultaneous inhibition of both enzymes should result in an improved antiparasitic effect.<sup>31,32</sup> MTX (a well-known DHFR inhibitor) is a potent inhibitor of TbDHFR ( $K_i = 15$  nM)<sup>33,34</sup> that exerts an inhibitory activity also against recombinant TbPTR1

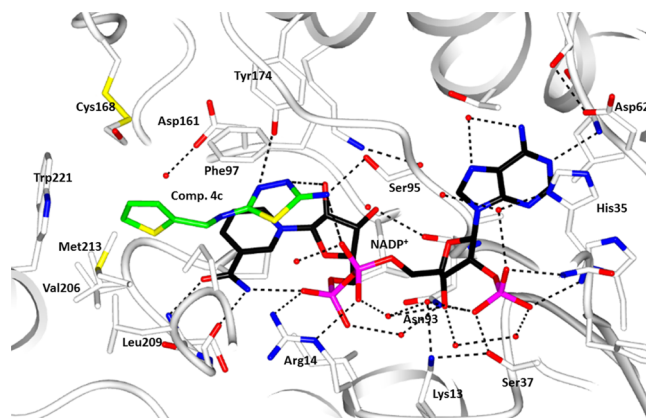


**Figure 5.** Noncovalent interactions involving inhibitor **4c** (green sticks) in the TbPTR1 active site. The **4c** thiadiazole ring is sandwiched between the nicotinamide ring of the NADP<sup>+</sup> cofactor and the phenyl ring of Phe97, as for compounds **I**, **II**, and **III**. H-bonds are represented by black dashed lines; water molecules are shown as red spheres. All model atoms are color coded following atom types, except C atoms for protein residues are in white, for NADP<sup>+</sup> in black, and for the inhibitor in green. The protein backbone is drawn as a white cartoon. Note the modified Cys168 as S,S-(2-hydroxyethyl)thiocysteine (CME). Interaction distances are reported in Table S2.1 in the Supporting Information.

( $K_i = 50$  nM). In standard *T. brucei* growth conditions, as in our experiments, where the media is supplemented with 9 μM folic acid, MTX is a poor antitrypanocidal agent showing an EC<sub>50</sub> of 35 ± 3.0 μM, 1000 times higher than the reported EC<sub>50</sub> of 0.012 μM with no folate supplementation.<sup>35–37</sup>

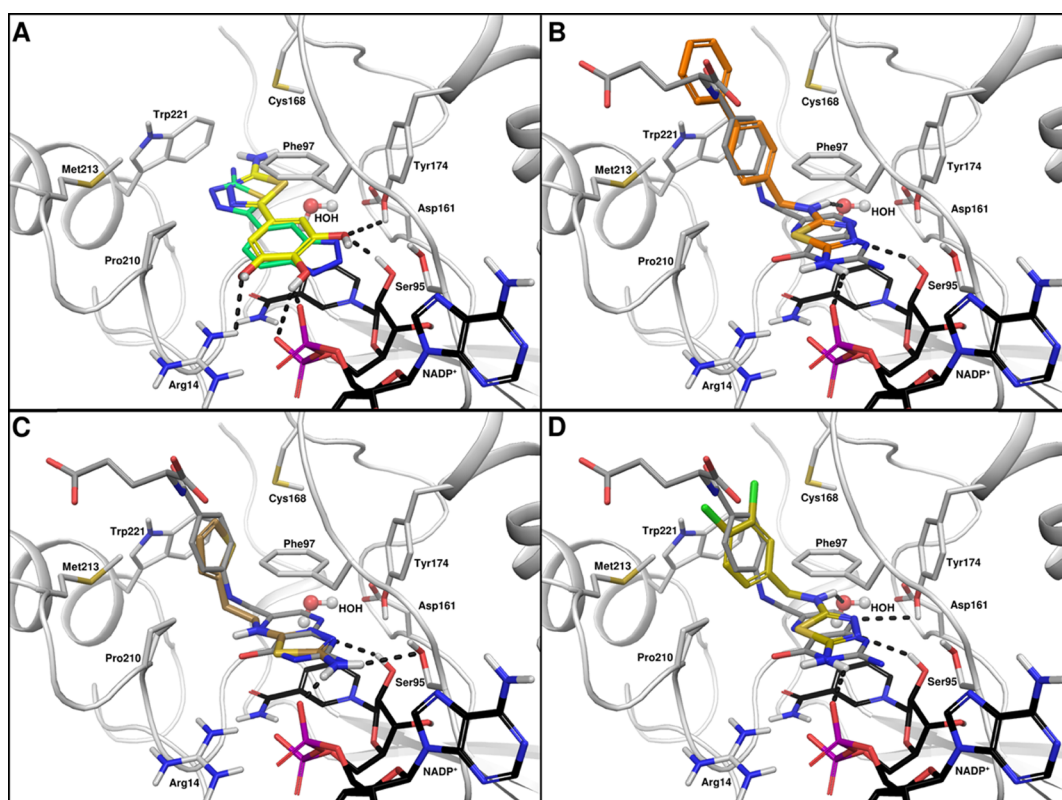


**Figure 6.** Docking poses of compounds in *TbPTR1*. The reference crystal structure (PDB ID 2X9G) of *TbPTR1* is shown in cartoon representation, with important interacting residues in stick representation with gray carbons in complex with NADP<sup>+</sup> (stick representation, black carbons). (A) Docked pose of compound **1f** (sticks, yellow carbons, 2x9g-1f\_dockedcomplex.pdb in [Supporting Information](#)) shown with the crystallographic orientation of compound **IV** (from PDB ID 4WCD, pale turquoise carbons) for reference. (B–D) Sample docking poses of compound **4m** (sticks, orange carbons, 2x9g-4m\_dockedcomplex.pdb in [Supporting Information](#)), **4o** (sticks, brown carbons, 2x9g-4o\_dockedcomplex.pdb in [Supporting Information](#)), and **4e** (sticks, golden carbons, 2x9g-4e\_dockedcomplex.pdb in [Supporting Information](#)) with folate from PDB ID 3BMC (sticks, dark gray carbons) shown for reference. Hydrogen bonds are indicated by black dotted lines.

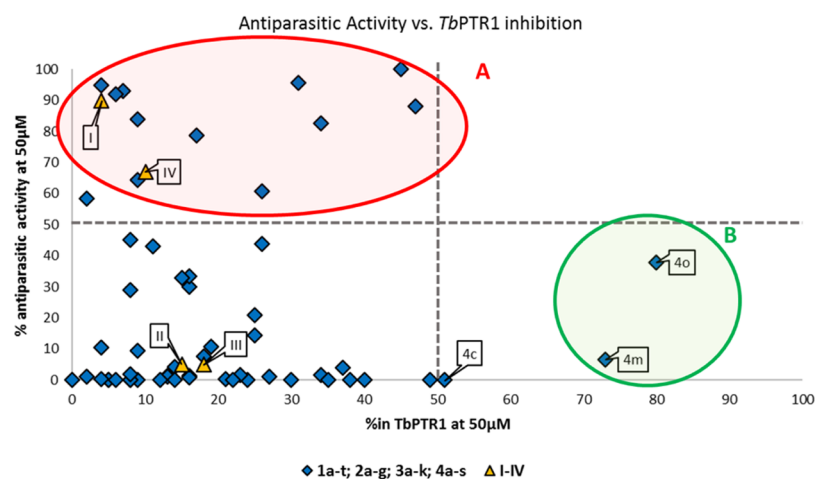


**Figure 7.** Correlation between the percentage of enzyme inhibition of the target *TbPTR1* at 50  $\mu\text{M}$  and antiparasitic activity against *T. brucei* performed at the same concentration. (A) Thiadiazoles that showed antiparasitic activity with  $\text{EC}_{50}$  in the range of 0.8–58.0  $\mu\text{M}$  but poor efficacy against the target enzyme. (B) Compounds **4m** and **4o**, which showed *TbPTR1* inhibition but poor antiparasitic activity as single agents.

We compared the antiparasitic activity of some selected *TbPTR1* inhibitors as single agents and in combination with MTX, resulting in the selection of four compounds that presented distinct *TbPTR1* inhibition (**4m**,  $\text{IC}_{50} = 16 \mu\text{M}$ ; **4o**,  $\text{IC}_{50} = 25 \mu\text{M}$ ; **4h**,  $\text{IC}_{50} = 70 \mu\text{M}$ , and **3k**,  $\text{IC}_{50} > 70 \mu\text{M}$ ), and dose–response antiparasitic studies were performed. Compounds **1m**, **2d**, and **2e** were associated with 34–48%

antiparasitic activity at 50  $\mu\text{M}$ , whereas all other compounds yielded <30% antiparasitic activity. Therefore, the entire compound library was considered associated with low activity against *T. brucei* (Figure S3, [Supporting Information](#)). The *TbPTR1* inhibitors were combined with equimolar amounts of MTX (the  $\text{EC}_{50}$  value for MTX against *T. brucei* was  $35 \pm 3.0 \mu\text{M}$ ), and dose–response curves were determined (Figure 8).

The data show a measurable antiparasitic  $EC_{50}$  for the combinations and, in particular, the  $EC_{50}$  of MTX was reduced by a factor of 4.1 when combined with **4m** ( $EC_{50}$   $8.6 \pm 1.1 \mu\text{M}$ , Figures 8 and S4) and by a factor of 2 when combined with **4o** ( $EC_{50}$   $17.5 \pm 0.5 \mu\text{M}$ , Figures 8 and S4). Interestingly, only compounds showing *Tb*PTR1 inhibition (**4m** and **4o**) were able to potentiate MTX  $EC_{50}$ . Although MTX can inhibit both PTR1 and DHFR enzymes, the observed potentiation effect can arise from the enhancement of the dual inhibitory effect caused by supplementary PTR1 inhibition induced by the thiadiazoles used in the combination. In fact, despite the PTR1 inhibitory activity, the administration of  $50 \mu\text{M}$  of **4m** alone did not show any significant antiparasitic effect. Similarly, compounds **4o** and **4c** showed low *T. brucei* cell inhibitory activity. In addition, an increasing concentration of **4m** induced an increasing inhibitory effect of MTX in combination, indicating that potentiation occurs. This potentiation is greater than the simple additive effect (**4m** has no intrinsic antiparasitic activity); therefore, the potency of the combination is much greater than the potency of the single agents that compose it.

On the basis of these results, we expected to rescue the DHFR activity and consequently, parasite vitality, by supplementing with folic acid, the natural substrate of DHFR. Our compounds display almost no inhibition of DHFR (Table S3). It is reported that folic acid competes with MTX for DHFR, displacing it and reversing DHFR inhibition on a cellular level.<sup>38</sup> Folic acid supply is in fact used in clinical settings to alleviate the toxicity of MTX.<sup>39,40</sup> We observed the same behavior in *T. brucei* cell culture. After testing different folic acid concentrations, we observed that the addition of 1 mM folic acid was able to reduce the antiparasitic activity of MTX alone, safeguarding the cell survival, without interfering with parasite growth (Figure 9A). Focusing on compound **4m**, which showed the best *Tb*PTR1  $IC_{50}$  value and potentiation of the antiparasitic activity of MTX, we observed that supplementation with 1 mM folic acid was able to rescue cell growth treated with **4m** and MTX (Figure 9B). Our

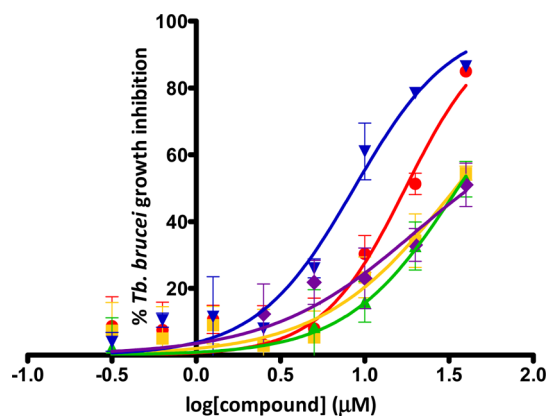


**Figure 8.** Dose–response curves for *T. b. brucei* growth inhibition for compounds **4m** (in blue), **4o** (in red), **4h** (in green), and **3k** (in yellow) in combination with equimolar amounts of MTX. The dose–response curve for MTX alone is reported in purple ( $EC_{50} = 35 \pm 3.0 \mu\text{M}$ ). From the dose–response curve, a measurable antiparasitic  $EC_{50}$  for the four tested compounds (**4m**,  $EC_{50} = 8.6 \pm 1.1 \mu\text{M}$ ; **4o**,  $EC_{50} = 17.5 \pm 0.5 \mu\text{M}$ ; **4h**,  $EC_{50} = 35.6 \pm 5.8 \mu\text{M}$ ; and **3k**,  $EC_{50} = 34.5 \pm 3.2 \mu\text{M}$ ) was extrapolated. The dose–response curves are the merged curves from at least two independent data sets done in triplicate, whereas the  $EC_{50}$  value in brackets represents the arithmetic average ( $\pm$  standard deviation) of at least two independent assays.

data suggest that PTR1 inhibitors potentiate the antiparasitic effect of MTX, probably by preventing the PTR1 bypass for the reduction of folate.

Folic acid administration reverses the effect of MTX (by binding both to DHFR and PTR1) up to almost the original activity of MTX alone, but does not abrogate the effect of MTX completely. This nonphysiological folate concentration could reduce the antitrypanosomal potency of MTX through competition for drug uptake.<sup>36</sup> Thus, the low effect of MTX on the parasite cells is due to a low amount of compound passing into the cells, and as a consequence, there is a low amount of MTX inside the cells and low inhibition of *Tb*PTR1 and *Tb*DHFR. Instead the trans-membrane crossing of **4m** and **4o** is different from that of MTX because they have a folate-unrelated structure. This allows **4m** to be competitive with respect to MTX in the binding toward PTR1. Therefore, coadministering the thiadiazole with MTX, the compound is delivered to the cell and is available to induce supplementary inhibition on PTR1, thus causing an overall potentiation effect. More experiments are ongoing to clarify the potentiation effect of PTR1 inhibitors using other classes of PTR1 inhibitors.

**Early Compound-Mediated Toxicity and Liability Studies.** Independent of the effect of any antiparasitic potential of compounds, they were evaluated using a panel of early-toxicity assays comprising cytotoxicity (A549, human lung adenocarcinoma epithelial cell line and WI-38, human lung fibroblasts), mitochondrial toxicity (786-O, human renal carcinoma cell line), *h*ERG inhibition,<sup>31</sup> cytochrome P450 inhibition (CYP1A2, CYP2C9, CYP2C19, CYP2D6, and CYP3A4),<sup>31</sup> and Aurora B kinase inhibition. These experiments were performed using  $10 \mu\text{M}$  of each compound and the output was expressed as % inhibition, which is displayed as a heat map in Figure 10. An acceptable profile for compounds at this stage in the drug-discovery process should exhibit  $<30\%$  inhibition at  $10 \mu\text{M}$  in the case of mitochondrial toxicity, *h*ERG, CYP isoforms, and Aurora B kinase, whereas the percentage of A549/WI-38 cell growth should be  $>70\%$ .<sup>32</sup> Almost all evaluated compounds (series 1–3) showed a safe profile, revealing that the thiadiazole scaffold has a well-tolerated liability profile that can be further explored during their development. Some compounds in series 4 showed a liability risk for their effects on *h*ERG, CYP2D6, and WI-38 cells, which appears to be due to the introduction of the second nitrogen atom that can induce a toxic effect on the thiadiazole core. The cytotoxicity of the compounds selected for combination studies (**4m**, **4o**, **3k**, **4h**) at  $100 \mu\text{M}$  alone and in combination with equimolar MTX was evaluated using THP-1 macrophage-like cells. Notably, no increase in toxicity was seen in THP-1 cells for compound **4m** (Figure 11). For the two compounds active against *Tb*PTR1 (**4m** and **4o**),  $IC_{50}$  against *h*ERG, cytochrome P450, and mitochondrial toxicity were determined (reported in Supporting Information). We observed that the dose of compounds **4m**, **4o**, **4c**, and **3k** was  $4 \mu\text{M}$  in the potentiation assays. Therefore, considering the toxicity of the compounds at  $10 \mu\text{M}$ , we can extrapolate that only CYP1A2 shows around 50% of inhibition at  $4 \mu\text{M}$  in the combination studies. In the case of *h*ERG, CYP2D6, CYP2A9, CYP2C19, and mitochondrial toxicity, there is a selectivity index of around 3–4 fold, thus showing an acceptable profile.

## CONCLUSIONS

In the present work, we have established an efficient platform to identify and characterize hits for further development toward the discovery of more potent antitrypanosomatidic agents. A

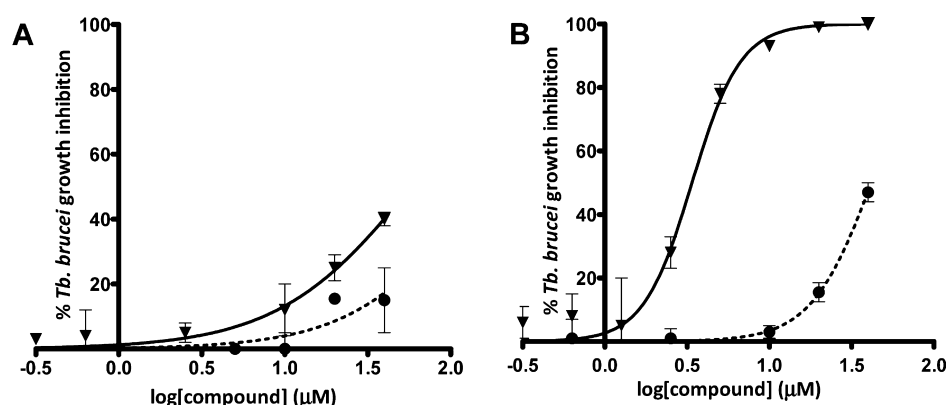


**Figure 9.** Effect of 1 mM folic acid (circles and dashed line) on *T. b. brucei* growth inhibition induced by MTX (A, reverse triangle and filled line) or the equimolar combination of **4m** + MTX (B, reverse triangle and filled line). The depicted dose–response curves are the merged curves from at least two independent assays.

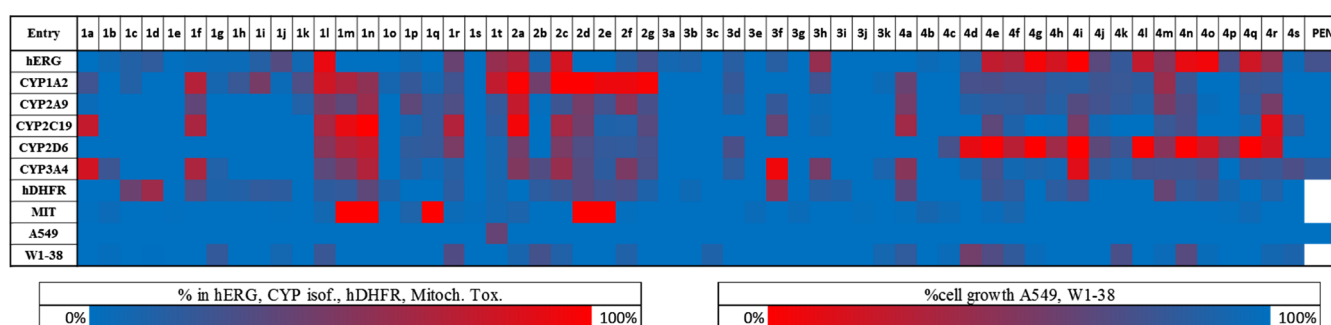


**Figure 10.** Summary heat map of the in vitro assays to determine possible liability issues for all synthesized compounds. Assays were performed to assess inhibition of *hERG* and five CYP isoforms (1A2, 2C9, 2C19, 2D6, and 3A4), growth inhibition of A549 and W1-38 cell lines, and mitochondrial toxicity at 10  $\mu\text{M}$ . The *hDHFR* inhibition was determined at 100  $\mu\text{M}$ . The data, expressed as percentage values, were organized by adopting a color code for rapid and intuitive visualization. The ideal compound should have all tiles blue, indicating a safe toxicological profile for progressing into the development pipeline. The cells are colored from blue (100% of cell growth at the tested concentration) to red (0% of cell growth at the tested concentration) for A549 and W1-38 and from blue (0% of inhibitory activity at the tested concentration) to red (100% of inhibitory activity at the tested concentration) for CYP isoforms, *hERG*, *hDHFR*, and mitochondrial toxicity.

crystallization screen with a library of previously identified inhibitors of *LmPTR1* with a thiadiazole scaffold was performed, and it resulted in structures of four new *TbPTR1*-cofactor-inhibitor complexes, which guided the design of new thiadiazoles in a structure-based approach. Compounds were synthesized and evaluated for inhibitory activity against *TbPTR1* and for antiparasitic activity in a phenotypic assay against *T. brucei*. Two of the best compounds yielded  $\text{IC}_{50}$  values of 16 and 25  $\mu\text{M}$  against *TbPTR1* and share a 2,5-diamino-1,3,4-thiadiazole scaffold. Compound **4c**, a representative of this class, was successfully crystallized in a ternary complex with *TbPTR1* (*TbPTR1*– $\text{NADP}^+$ –**4c**), supporting the binding mode of the earliest compounds (I–III). With respect to our starting compounds, I–IV, we have improved the compounds' biological profiles, with 23 out of 57 compounds displaying a better *PTR1* inhibition profile. Five compounds showed a better antiparasitic effect with respect to I and IV.

In previous experiments performed on *LmPTR1* thiadiazole inhibitors, we have shown the combination effect with pyrimethamine on promastigotes of *L. infantum* and *mexicana*. This work specifically addressed the ability of *TbPTR1* inhibitors to potentiate the effect of the DHFR inhibitor MTX against *T. brucei* by performing studies in combination with compounds **3k**, **4h**, **4o**, and **4m**. The potentiating effect was observed only with the compounds inhibiting *TbPTR1*, **4o** and **4m**. In particular, we focused on compound **4m**, which showed the greatest inhibition

against the target enzyme, *TbPTR1*. When combined with MTX, the  $\text{EC}_{50}$  of MTX against *T. brucei* improved 4.1 times ( $\text{EC}_{50}$  MTX alone 35  $\mu\text{M}$ ;  $\text{EC}_{50}$  MTX and **4m** 8.6  $\mu\text{M}$ ). No increase in the toxicity of the *PTR1*–DHFR inhibitor combination with respect to the single compounds was observed. In addition, we demonstrated that the potentiation activity of a *PTR1* inhibitor combined with MTX could be reversed through administration of folic acid, the natural substrate of DHFR. The molecular mechanism that might explain this reversal of inhibition is likely complex and will be studied in future work. By adopting an efficient early hit discovery platform, we showed that the 2-amino-1,3,4-thiadiazole scaffold can be considered a promising approach for the development of anti-*T. brucei* agents targeting *TbPTR1*. Whereas the compounds show modest  $\text{IC}_{50}$  values against both the enzymes and parasites in isolation, our results suggest that combining the *PTR1* inhibitors with DHFR inhibitors provides a valid strategy for developing more potent antiparasitic agents.

## EXPERIMENTAL SECTION

**Synthetic Chemistry.** The chemical procedures and characterization of all synthesized compounds and the respective intermediates are reported in the Supporting Information.

**X-ray Crystallography.** *TbPTR1*-cofactor-inhibitor complexes with I and II were prepared by incubating protein (6 mg/mL, 1 mM NADPH, 10 mM dithiothreitol) with 2.5  $\mu\text{L}$  of a 5

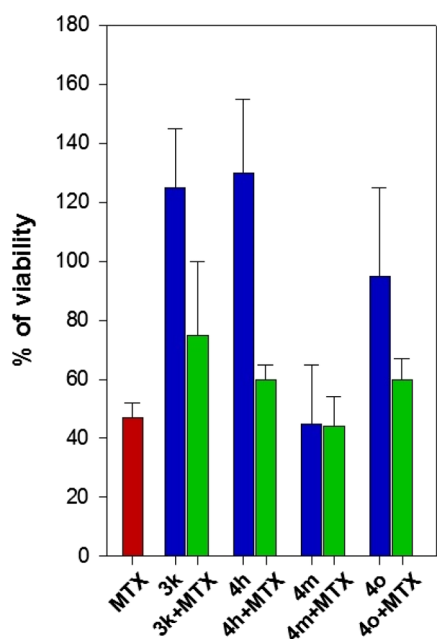


**Figure 11.** Toxicity against THP-1 cells for selected thiadiazoles **3k**, **4h**, **4m**, and **4o** (in blue), MTX (in red), and equimolar combinations of thiadiazoles and MTX at 100  $\mu$ M (in green). The data presented are the average  $\pm$  standard deviation from at least two independent experiments.

mM solution of inhibitor in dimethylsulfoxide (DMSO) in 20 mM Tris-HCl pH 7.5 on ice for 1 h before crystallization. Hanging drops (1.5  $\mu$ L of protein solution and 1.5  $\mu$ L of reservoir) were incubated over 1 mL of reservoir (2.7 M sodium acetate, 10 mM sodium citrate pH 4.5). Crystals grew at 20  $^{\circ}$ C in a few days. Complexes with compounds **III**, **IV**, and **4c** were obtained by soaking the preformed crystals of a *TbPTR1*-cofactor binary complex obtained in sitting drops equilibrated against reservoir (1.5–2.5 M sodium acetate and 100 mM sodium citrate pH 5.0). The crystals were soaked for 4–6 h in the crystallization buffer containing 2–4 mM of each compound dissolved in DMSO (without exceeding a DMSO/crystal solution ratio of 1:9). The crystals were transferred in a cryoprotectant (precipitant plus 30% glycerol) and flash-frozen in liquid nitrogen or taken directly from mother liquor and flash-cooled. Data were recorded using a Rigaku MicroMax 007 rotating anode and an R-Axis IV<sup>++</sup> dual image plate detector system at the European Synchrotron Radiation Facility (Grenoble, France) on beamline BM30A with an ADSC Q315r detector, at the Diamond Light Source (Didcot, UK) on beamline I04 with a PILATUS 6M-F detector, or at the Elettra Synchrotron (Trieste, Italy) on beamline XRD1 with a PILATUS 2M detector. Data were processed with MOSFLM<sup>41</sup> or XDS<sup>42</sup> and then scaled with SCALA<sup>43</sup> with the CCP4 software suite.<sup>44</sup> The structures were solved by molecular replacement<sup>45</sup> using *TbPTR1* (PDB: 2X9G) as the starting model.<sup>27</sup> Rigid body refinement and rounds of restrained refinement were carried out using REFMAC5.<sup>46</sup> Inspection of electron density, model manipulation, and identification of solvent, ions, and ligands were done using COOT.<sup>47</sup> Figures were generated with CCP4mg.<sup>48</sup> The coordinates and structure factors were deposited in the Protein Data Bank (PDB) under accession codes 2YHI, 2YHU, 4WCD, 4WCF, and 5IZC for compounds **I**, **II**, **III**, **IV**, and **4c**, respectively. In *TbPTR1*-**II** and *TbPTR1*-**III**,

Cys168 is chemically modified to S-oxycysteine (defined as CSX) indicative of a reactive cysteine (see Figure 2B,C).

**Computational Docking.** The three-dimensional (3D) structures of the compounds were created from SMILES strings and optimized with the OPLS\_2005 force field<sup>49</sup> using Maestro (Schrödinger, LLC).<sup>50</sup> Ligand preparation included the generation of stereoisomers (up to eight) and low-energy ring conformations (one per compound) as well as determination of ionization states and tautomers for pH 7.0  $\pm$  0.5 using Epik. Highly conserved structural water was identified by the WatCH clustering approach.<sup>51</sup> Briefly, 99 chains from *TbPTR1* crystal structures (see Table S5 for a list of structures) were superimposed, and their crystallographic water positions were clustered with a distance criterion of 2.4  $\text{Å}$  for considering identical water oxygen positions. Seventeen water sites with at least 50% conservation were considered to be conserved. *TbPTR1* receptors for docking and SiteMap analysis<sup>52</sup> were composed of chain A of the respective crystal structure and a C-terminal tripeptide from the neighboring subunit, Val266 to Ala268, pointing into the active site of chain A. Crystallographic solvent molecules were removed and replaced with conserved water molecules (from WatCH clustering) for docking studies. SiteMap calculations were conducted with PDB IDs 2YHI, 2YHU, 4WCD, and 4WCF. Docking was carried out to PDB ID 2X9G.<sup>27</sup> Bond-order assignment and hydrogen atom addition was done with PrepWizard.<sup>49</sup> N- and C-termini of chain A were capped with N-acetyl and N-methyl amide groups, respectively. The NADP<sup>+</sup> cofactor protonation state was computed at pH 7.0  $\pm$  0.5. Protein protonation states were assigned for pH 7.0 using PROPKA.<sup>53</sup> The H-bond network was optimized, and all hydrogens were subjected to a restrained minimization. For the SiteMap analysis, the site was defined by the thiadiazole core moiety of the ligand. A surrounding region of 3  $\text{Å}$  was examined. Ten site points were required per reported site, and site maps were cropped at 3  $\text{Å}$  from their nearest site point. Otherwise, standard values were used. For docking, a 20  $\text{Å}$   $\times$  20  $\text{Å}$   $\times$  20  $\text{Å}$  docking grid was centered on Phe97. The hydroxyl groups of Ser95, Cys168, Tyr174, and NADP<sup>+</sup> ribose were set rotatable. Docking was performed with Glide (Schrödinger, LLC)<sup>54–56</sup> using the SP protocol (standard precision). The maximum ligand size and rotatable bond count were kept at standard values. A scaling factor of 0.80 for the ligand van der Waals radii and a partial charge cutoff of 0.15 were used. Ligands were treated as flexible, nitrogen inversions, and ring conformations were sampled. Nonplanar conformations were penalized when performing bias sampling of amide torsions. Epik state penalties were added to the docking score; intramolecular hydrogen bonds were rewarded; and conjugated  $\pi$  group planarity was enhanced. Twenty poses per ligand were subjected to postdocking energy minimization, employing a pose rejection threshold of 0.5 kcal/mol. Up to 10 final solutions were collected.

The validation of the docking protocol was based on cross-docking studies of the crystallized compounds **I**, **II**, **III**, **IV**, and **4c**. As shown in Table S6 and as discussed in the “Docking Validation section” of the Supporting Information, near-native poses were overall reproduced with the current protocol and typically found within 0.3 kcal/mol of the best-scoring docking solution, as ranked by the docking score. Poses were therefore ranked by the Glide docking score, and all poses within 1.0 kcal/mol of the top scoring solution were further analyzed. A visual inspection of the interaction pattern and comparison with crystal structures 3BMC (*TbPTR1* in complex with folate) and 5IZC (*TbPTR1* in complex with **4c**) were used to select the most likely

poses on the basis of experimental evidence. Docking results are also given in Table S7 in the [Supporting Information](#).

#### Biological Assays. Protein Expression and Purification.

*TbPTR1*, *LmPTR1*, *TbDHFR*, *LmDHFR*, and *hDHFR* were obtained and purified as reported in our previous work.<sup>32</sup> The kinetic characterization ( $K_m$  and  $k_{cat}$ ) of the enzymes is reported in Table S8 of the [Supporting Information](#).

***TbPTR1*, *LmPTR1*, *TbDHFR*, *LmDHFR*, and *hDHFR* Enzyme Assays.** The thiadiazoles were a small part of a library of many thousands of molecules that we tested within the three-year European project NMTrypI (<http://fp7-nmtrypi.eu>). Because of the sharing of technologies within the NMTrypI platform, we were able to perform the enzymatic studies against *TbPTR1* and *LmPTR1* and the early-toxicity assays by HTS methodologies. The in vitro assays used in the current study were based upon those reported in the literature, and the kinetic data are comparable (Table S8).<sup>34</sup> Because PTR1 enzymes use  $H_2B$  as a substrate and also require NADPH for the reaction, the reduction of  $H_2B$  to  $H_4B$  by PTR1 is nonenzymatically linked with the reduction of cytochrome *c* in this assay, which is detected at 550 nm. The formation of cyt *c*  $Fe^{2+}$  results in a signal increase in the photometric readout.

*TbPTR1* and *LmPTR1* activities were assayed in a buffer containing 20 mM sodium citrate (pH 6.0). The final reaction mixture contained the test compound in a range of concentrations and *TbPTR1/LmPTR1* (6.0 nM/12.0 nM),  $H_2B$  (0.3  $\mu M$ /3.0  $\mu M$ ), cytochrome *c* (100  $\mu M$ /100  $\mu M$ ), and NADPH (500  $\mu M$ /500  $\mu M$ ). The final assay volume was 50  $\mu L$  in 384-well clear plates (Greiner Bio-One, 781101). Compound screening was performed by addition of the compound to assay plates (in 100% DMSO), followed by addition of 45  $\mu L$  reaction mix (enzyme,  $H_2B$ , and cytochrome *c* in 20 mM sodium citrate buffer). A pre-read was made at 550 nm using an EnVision Multilabel Reader 2103 (PerkinElmer Inc, US), followed by incubation of the assay plates at 30 °C for 10 min. The reaction was initiated by addition of 5  $\mu L$  of NADPH (from a stock at 5 mM in ultrapure water), followed by kinetically reading the assay plates at 550 nm using the EnVision Multilabel Reader at 10, 20, 30, 40, and 50 min and calculating the slope of the reaction in each well. The screening data were analyzed using ActivityBase (IDBS), and for outlier elimination in the control wells, the 3-sigma method was applied. On the basis of the slope, data were normalized to the positive control MTX for *TbPTR1/LmPTR1* (1  $\mu M$ /50  $\mu M$ , yielding 100% inhibition) and negative controls (1% DMSO, yielding 0% inhibition), and % inhibition was calculated for all samples. The measurement at time 0 min was used to flag the interfering samples. Each compound was tested in triplicate, and the  $pIC_{50}$  value, standard deviation, Hill slope, and minimum signal and maximum signal for each dose–response curve were obtained using a four-parameter logistic fit in the XE module of ActivityBase (IDBS). Compounds displaying a percentage of inhibition against *TbPTR1* above 30% at 50  $\mu M$  were further analyzed at concentrations from 0.001 to 100  $\mu M$  for the determination of  $IC_{50}$ . The  $IC_{50}$  value of pyrimethamine ( $IC_{50} = 0.09 \mu M$  against *TbPTR1*), a DHFR inhibitor also able to inhibit PTR1, was measured routinely as a standard. However, not all compounds selected gave measurable  $IC_{50}$  in the dose–response assays. *LmDHFR*, *TbDHFR*, and *hDHFR* activities were assessed spectrophotometrically as previously described, and the values for the kinetic constants characterizing each enzyme ( $K_m$ ) were comparable to literature values (Table S8).<sup>22</sup>

***hERG* Cardiotoxicity Assay.** This assay made use of Invitrogen's Predictor *hERG* fluorescence polarization (FP) assay. The assay uses a membrane fraction containing the *hERG* channel (Predictor *hERG* membrane) and a high-affinity red fluorescent *hERG* channel ligand or "tracer" (Predictor *hERG* Tracer Red), whose displacement by test compounds can be determined in a homogenous, FP-based format.<sup>32</sup>

**Cytochrome P450 1A2, 2C9, 2C19, 2D6, and 3A4 Assays.** These assays made use of the Promega P450-Glo assay platform. Each CYP450 assay made use of microsomal preparations of cytochromes from baculovirus-infected insect cells. Action of the CYP450 enzymes on each substrate ultimately resulted in the generation of light, and a decrease in this was indicative of inhibition of the enzyme.<sup>32</sup>

**Cytotoxicity Assay against A549 and W1-38 Cells.** The assays were performed using the CellTiter-Glo assay from Promega. The assay detects cellular ATP content, with the amount of ATP being directly proportional to the number of cells present. The A549 cells were obtained from DSMZ (German Collection of Microorganisms and Cell Cultures, Braunschweig, Germany) and W1-38 cells were obtained from ATCC (ATCC CCL-75) and were grown in Dulbecco's modified Eagle medium (DMEM) with fetal calf serum (FCS) (10% v/v), streptomycin, (100  $\mu g/mL$ ) and penicillin G (100 U/mL).<sup>32</sup>

**Assessment of Mitochondrial Toxicity.** This assay made use of MitoTracker Red chloromethyl-X-rosamine (CMXRos) uptake and high content imaging to monitor compound-mediated mitochondrial toxicity in the 786-O (renal carcinoma) cell line. Cells were maintained using the Roswell Park Memorial Institute (RPMI)-1640 medium containing 2 mM glutamine, FCS (10% v/v), streptomycin (100  $\mu g/mL$ ), and penicillin G (100 U/mL).<sup>32</sup>

**In Vitro Evaluation of Activity against *T. brucei*.** The assay relies on indirect determination of parasite population viability by quantification of total DNA present in the well using the SYBR Green I DNA fluorescent dye. Briefly, the assay consisted of incubating bloodstream forms of the *T. b. brucei* Lister 427 strain in the presence of compounds for 72 h, followed by cell lysis and addition of the SYBR Green I dye.<sup>57</sup> Pentamidine at 120 nM was used as the reference compound showing an  $EC_{50}$  of  $3.8 \pm 0.48$  nM comparable with the value reported in the literature.<sup>58</sup> DMSO-treated parasites were used as negative controls and pentamidine-treated parasites and blank wells (without parasites) were used as positive controls. Compounds and controls were plated in a semiautomated process that utilizes the liquid handler Janus MDT (PerkinElmer), which is equipped with a 384 pipetting head capable of dispensing a minimum volume of 0.5  $\mu L$ . As *T. b. brucei* is sensitive to DMSO and tolerates a maximum of approximately 1% DMSO, compound libraries dissolved in 100% DMSO must be diluted at least 200-fold with the aid of "intermediate plates". Following compound plating in the final assay plate, 50  $\mu L$  of a parasite suspension at 8000 trypanosomes/mL was seeded to the assay and control plates and incubated for 72 h at 37 °C and 5%  $CO_2$ . At the assay endpoint, 15  $\mu L$  of the lysis solution (30 mM Tris-HCl pH 7.5, 7.5 mM EDTA, 0.012% saponin, and 0.12% Triton X-100) was added to the plates containing 0.5  $\mu L$  of SYBR Green I (10 000 $\times$ , Life Technologies) per 1 mL of lysis solution. The plates were shaken for 30 s at 800 rpm in a MixMate (Eppendorf) and incubated for 1 h in the dark at room temperature. The plates were then read for fluorescence at the microplate reader EnVision (PerkinElmer). Compounds that yielded >80% inhibition of parasite growth at 50  $\mu M$  were selected for  $EC_{50}$



determinations. However, not all selected compounds gave reliable EC<sub>50</sub> data in the dose–response assay.

**In Vitro Evaluation of Activity against *T. brucei* for MTX Potentiation Assays and Folic Acid Supplementation Experiment.** *T. b. brucei* Lister 427 bloodstream forms were grown at 37 °C and 5% CO<sub>2</sub> in a complete HMI-9 medium, supplemented with 10% FCS and 100 UI/mL of penicillin/streptomycin. The cultures were diluted until a cell density of 2 × 10<sup>6</sup>/mL was reached. The efficacy of compounds against *T. brucei* bloodstream forms was evaluated using a modified resazurin-based assay previously described.<sup>46</sup> The compounds were prepared from a stock solution in 10 mM DMSO and diluted in HMI-9 (supplemented or not with 1 mM folic acid, Sigma-Aldrich) to 40 μM work solution (0.4% DMSO, with the DMSO limit in the assay being 0.4%). For the combination assays, 40 μM equimolar mixture was prepared using 20 μM test compound and 20 μM MTX. The 40 μM work solution was then used to perform serial dilutions (1:2) in a 96-well plate. Upon compound addition to the test plate, the mid-log bloodstream forms were added (100 μL) in complete HMI-9 medium (supplemented or not with 1 mM folic acid) at a final cell density of 1 × 10<sup>4</sup>/mL in a final well volume of 200 μL with a maximum DMSO concentration of 0.2%. Following incubation for 72 h at 37 °C and 5% CO<sub>2</sub>, 20 μL of 0.5 mM resazurin solution was added, and the plates were incubated further for 4 h under the same conditions. Fluorescence was measured at 540 and 620 nm excitation and emission wavelengths, respectively, using a Synergy 2 multi-mode reader (BioTek). The antitrypanosomatid effect was evaluated by the determination of the IC<sub>50</sub> value (concentration required to inhibit growth by 50%) and calculated by the nonlinear regression analysis using GraphPad Prism version 5.00 for Windows, GraphPad Software, San Diego, California, USA ([www.graphpad.com](http://www.graphpad.com)). It was not possible to analyze the combination of 4m with MTX by adopting an isobologram approach, as described by Chou.<sup>59</sup> This approach requires the use of both compounds at their EC<sub>50</sub> potency in the combination, which is impossible to be detected for compound 4m having no intrinsic antiparasitic activity as a single agent at the tested concentrations. Folic acid (1 mM) was chosen on the basis of the following experiments. The stock solution of 10 mM folic acid dissolved in NaOH solution was used to perform a dose–response curve with folic acid alone to evaluate the maximum amount we could use without compromising parasite growth due to pH modification of the media. The highest concentration that we could use was 1 mM without interfering with the parasite growth or significantly changing the pH of the media. The IC<sub>50</sub> values reported are the averages of the results obtained in at least two independent experiments. Pentamidine was used as the reference drug and internal control in all assays. The average pentamidine EC<sub>50</sub> for the assays was 2.28 ± 1.18 nM.

#### Cytotoxicity Assessment against THP-1 Macrophages.

The effect of compounds 3k, 4h, 4m, and 4o on THP-1-derived macrophages was assessed by the colorimetric MTT assay [3-(4,5-dimethylthiazol-2-yl)-2,5-diphenyl tetrazolium bromide]. Briefly, 1 × 10<sup>6</sup> THP-1 cells were differentiated into macrophages by addition of 20 ng/mL of phorbol-myristate 13-acetate (PMA, Sigma-Aldrich) for 18 h, followed by replacement with a fresh medium and further incubation for 24 h. The cells were incubated with compounds ranging from 100 to 3 μM after dilution in the RPMI complete medium containing a maximum amount of 1% DMSO. After incubation for 72 h at 37 °C and 5% CO<sub>2</sub>, the medium was removed and 0.5 mg/mL MTT solution was added. The plates were incubated for 4 additional hours to

allow viable cells to convert MTT into a purple formazan product. Solubilization of formazan crystals was achieved by addition of 2-propanol, and absorbance was read at 570 nm using a Synergy 2 multi-mode reader (BioTek). Cytotoxicity was evaluated by the determination of the CC<sub>50</sub> value (drug concentration that reduced the percentage of viable cells by 50%) and calculated by the nonlinear regression analysis using GraphPad Prism version 5.00 for Windows, GraphPad Software, San Diego, California, USA ([www.graphpad.com](http://www.graphpad.com)).

## ■ ASSOCIATED CONTENT

### 📄 Supporting Information

The Supporting Information is available free of charge on the ACS Publications website at DOI: 10.1021/acsomega.7b00473.

Full data for the synthetic procedures and characterizations biological evaluation (enzyme inhibition for PTR1 and DHFR, antiparasitic activity, and liability), crystallographic statistics, and additional details for docking studies (PDF)

Docking protocol (XLSX)

2x9g\_1f\_dockedcomplex (PDB)

2x9g\_1e\_dockedcomplex (PDB)

2x9g\_4i\_dockedcomplex (PDB)

2x9g\_4m\_dockedcomplex (PDB)

2x9g\_4n\_dockedcomplex (PDB)

2x9g\_4o\_dockedcomplex (PDB)

### Accession Codes

PDB code 2X9G was used for docking studies. Crystal structures of the ternary complexes of five compounds have been deposited with the following PDB accession codes: 2YHI (I); 2YHU (II); 4WCF (III); 4WCD (IV); and 5IZC (4c).

Molecular formulas for 1a–t, 2a–g, 3a–k, and 4a–s (in CSV format) and the <sup>1</sup>H NMR and <sup>13</sup>C NMR spectra scan pictures for 1a–t, 2a–g, 3a–k, and 4a–s are available free of charge via the Internet at [https://fp7h-synergy.h-its.org/data\\_files/227](https://fp7h-synergy.h-its.org/data_files/227).

## ■ AUTHOR INFORMATION

### Corresponding Authors

\*E-mail: [w.n.hunter@dundee.ac.uk](mailto:w.n.hunter@dundee.ac.uk). Phone: 0044-(0)-1382-385745 (W.N.H.).

\*E-mail: [stefano.mangani@unisi.it](mailto:stefano.mangani@unisi.it). Phone: 0039-0577-234255 (S.M.).

\*E-mail: [luca.costantino@unimore.it](mailto:luca.costantino@unimore.it). Phone: 0039-059-205-8572 (L.C.).

\*E-mail: [mariaapaola.costi@unimore.it](mailto:mariaapaola.costi@unimore.it), [costimp@unimore.it](mailto:costimp@unimore.it). Phone: 0039-059-205-8579 (M.P.C.).

### ORCID

Cecilia Pozzi: 0000-0003-2574-3911

Maria P. Costi: 0000-0002-0443-5402

### Present Addresses

§§Erika Nerini, FB Communication srl. Via Bonacini, 91, 41121 Modena (Mo).

|||The University of Edinburgh, Institute of Quantitative Biology, Biochemistry and Biotechnology, Edinburgh (P.A.M.M.).

⊥⊥Excelra Knowledge Solutions, Plot No. 79, IDA Mallapur, Nacharam, Hyderabad-500076, India (P.S.).

###Division of Innovation, Instituto Butantan, São Paulo—SP, 05503-900, Brazil (L.H.F.-J.).

### Author Contributions

The manuscript was written with the contributions of all authors. P.L., I.P., D.M.C., M.S.S., A.C.-d.-S., R.L., S.G., G.W., B.E., M.K.,

P.G., J.R., M.W., B.B., V.H., P.A.M.M., E.N., C.P., F.d.P., G.L., N.S., S.F., P.S., L.H.F.-J., C.B.M., B.S.P., L.M.A., C.P.B., V.F., U.W., W.M., R.C.W., S.M., L.C., and M.P.C. belong to the FP7 European project "New Medicines for Trypanosomatid Infections", grant agreement no. 603240, <http://fp7-nmtrypi.eu>. P.L. and A.D. contributed equally to the work and are considered as cofirst authors.

### Funding

This project has received funding from the European Union's Seventh Framework Programme for Research, Technological Development, and Demonstration under grant agreement no. 603240 (NMTrypI-New Medicines for Trypanosomatid Infections). We acknowledge, in addition, the financial support of the European Community's Seventh Framework Programme (FP7/2007-2013) under BioStruct-X (grant no. 283570) to W.N.H., MIUR-PRIN2012 N° 2012 74BNKN\_003 to M.P.C. and the Wellcome Trust (grant nos. 801897, 094090) to W.N.H. I.P. and R.C.W. gratefully acknowledge the support of the Klaus Tschira Foundation.

### Notes

The authors declare no competing financial interest.

## ACKNOWLEDGMENTS

We acknowledge support and data collection facilities at the Diamond Light Source, the European Synchrotron Radiation Facility, and the Elettra Synchrotron. We acknowledge the COST Action CM1307, [http://www.cost.eu/COST\\_Actions/cmst/CM1307](http://www.cost.eu/COST_Actions/cmst/CM1307) for the contribution to the discussion of the research results.

## ABBREVIATIONS

WHO, World Health Organization; NTDs, neglected tropical diseases; HAT, human African trypanosomiasis; DHFR, dihydrofolate reductase; *TbPTR1*, *Trypanosoma brucei* pteridine reductase-1; MTX, methotrexate; *L. infantum*, *Leishmania infantum*; *T. brucei*, *Trypanosoma brucei*; *hERG*, human ether-a-go-go-related gene; THP-1, human monocytic cell line

## REFERENCES

- (1) Mackey, T. K.; Liang, B. A.; Cuomo, R.; Hafen, R.; Brouwer, K. C.; Lee, D. E. Emerging and Reemerging Neglected Tropical Diseases: A Review of Key Characteristics, Risk Factors, And the Policy and Innovation Environment. *Clin. Microbiol. Rev.* **2014**, *27*, 949–979.
- (2) Stuart, K.; Brun, R.; Croft, S.; Fairlamb, A.; Gürtler, R. E.; McKerrow, J.; Reed, S.; Tarleton, R. Kinetoplastids: Related Protozoan Pathogens, Different Diseases. *J. Clin. Invest.* **2008**, *118*, 1301–1310.
- (3) Brun, R.; Blum, J.; Chappuis, F.; Burri, C. Human African Trypanosomiasis. *Lancet* **2010**, *375*, 148–159.
- (4) Alirol, E.; Schrupf, D.; Heradi, J. A.; Riedel, A.; De Patoul, C.; Quere, M.; Chappuis, F. Nifurtimox-Eflornithine Combination Therapy for Second-Stage Gambiense Human African Trypanosomiasis: Médecins Sans Frontières Experience in the Democratic Republic of the Congo. *Clin. Infect. Dis.* **2013**, *56*, 195–203.
- (5) Kuepfer, I.; Schmid, C.; Allan, M.; Edielu, A.; Haary, E. P.; Kakembo, A.; Kibona, S.; Blum, J.; Burri, C. Safety and Efficacy of the 10-Day Melarsoprol Schedule for the Treatment of Second Stage Rhodesiense Sleeping Sickness. *PLoS Neglected Trop. Dis.* **2012**, *6*, No. e1695.
- (6) Gilbert, I. H. Drug Discovery for Neglected Diseases: Molecular Target-Based and Phenotypic Approaches. *J. Med. Chem.* **2013**, *56*, 7719–7726.
- (7) Jacobs, R. T.; Nare, B.; Phillips, M. a. State of the Art in African Trypanosome Drug Discovery. *Curr. Top. Med. Chem.* **2011**, *11*, 1255–1274.

(8) Bowyer, P. W.; Tate, E. W.; Leatherbarrow, R. J.; Holder, A. A.; Smith, D. F.; Brown, K. A. N-Myristoyltransferase: A Prospective Drug Target for Protozoan Parasites. *ChemMedChem* **2008**, *3*, 402–408.

(9) Van Voorhis, W. C.; Rivas, K. L.; Bendale, P.; Nallan, L.; Hornéy, C.; Barrett, L. K.; Bauer, K. D.; Smart, B. P.; Ankala, S.; Hucke, O.; Verlinde, C. L. M. J.; Chakrabarti, D.; Strickland, C.; Yokoyama, K.; Buckner, F. S.; Hamilton, A. D.; Williams, D. K.; Lombardo, L. J.; Floyd, D.; Gelb, M. H. Efficacy, Pharmacokinetics, and Metabolism of Tetrahydroquinoline Inhibitors of Plasmodium Falciparum Protein Farnesyltransferase. *Antimicrob. Agents Chemother.* **2007**, *51*, 3659–3671.

(10) Martyn, D. C.; Jones, D. C.; Fairlamb, A. H.; Clardy, J. High-Throughput Screening Affords Novel and Selective Trypanothione Reductase Inhibitors with Anti-Trypanosomal Activity. *Bioorg. Med. Chem. Lett.* **2007**, *17*, 1280–1283.

(11) Steverding, D.; Sexton, D. W.; Wang, X.; Gehrke, S. S.; Wagner, G. K.; Caffrey, C. R. *Trypanosoma Brucei*: Chemical Evidence That Cathepsin L Is Essential for Survival and a Relevant Drug Target. *Int. J. Parasitol.* **2012**, *42*, 481–488.

(12) Hawser, S.; Lociuero, S.; Islam, K. Dihydrofolate Reductase Inhibitors as Antibacterial Agents. *Biochem. Pharmacol.* **2006**, *71*, 941–948.

(13) Yuthavong, Y.; Yuvaniyama, J.; Chitnumsub, P.; Vanichtanankul, J.; Chusacultanchai, S.; Tarnchompoo, B.; Vilaivan, T.; Kamchonwongpaisan, S. Malarial (*Plasmodium Falciparum*) Dihydrofolate Reductase-Thymidylate Synthase: Structural Basis for Antifolate Resistance and Development of Effective Inhibitors. *Parasitology* **2005**, *130*, 249–259.

(14) Vickers, T. J.; Beverley, S. M. Folate Metabolic Pathways in *Leishmania*. *Essays Biochem.* **2011**, *51*, 63–80.

(15) Dawson, A.; Gibellini, F.; Sienkiewicz, N.; Tulloch, L. B.; Fyfe, P. K.; McLuskey, K.; Fairlamb, A. H.; Hunter, W. N. Structure and Reactivity of *Trypanosoma Brucei* Pteridine Reductase: Inhibition by the Archetypal Antifolate Methotrexate. *Mol. Microbiol.* **2006**, *61*, 1457–1468.

(16) Bello, A. R.; Nare, B.; Freedman, D.; Hardy, L.; Beverley, S. M. PTR1: A Reductase Mediating Salvage of Oxidized Pteridines and Methotrexate Resistance in the Protozoan Parasite *Leishmania Major*. *Proc. Natl. Acad. Sci. U.S.A.* **1994**, *91*, 11442–11446.

(17) Sienkiewicz, N.; Ong, H. B.; Fairlamb, A. H. *Trypanosoma Brucei* Pteridine Reductase 1 Is Essential for Survival in Vitro and for Virulence in Mice. *Mol. Microbiol.* **2010**, *77*, 658–671.

(18) Ong, H. B.; Sienkiewicz, N.; Wyllie, S.; Fairlamb, A. H. Dissecting the Metabolic Roles of Pteridine Reductase 1 in *Trypanosoma Brucei* and *Leishmania Major*. *J. Biol. Chem.* **2011**, *286*, 10429–10438.

(19) Spinks, D.; Ong, H. B.; Mpmahanga, C. P.; Shanks, E. J.; Robinson, D. A.; Collie, I. T.; Read, K. D.; Frearson, J. A.; Wyatt, P. G.; Brenk, R.; Fairlamb, A. H.; Gilbert, I. H. Design, Synthesis and Biological Evaluation of Novel Inhibitors of *Trypanosoma Brucei* Pteridine Reductase 1. *ChemMedChem* **2011**, *6*, 302–308.

(20) Tulloch, L. B.; Martini, V. P.; Iulek, J.; Huggan, J. K.; Lee, J. H.; Gibson, C. L.; Smith, T. K.; Suckling, C. J.; Hunter, W. N. Structure-Based Design of Pteridine Reductase Inhibitors Targeting African Sleeping Sickness and the Leishmaniases. *J. Med. Chem.* **2010**, *53*, 221–229.

(21) Cunningham, M. L.; Beverley, S. M. Pteridine Salvage throughout the *Leishmania* Infectious Cycle: Implications for Antifolate Chemotherapy. *Mol. Biochem. Parasitol.* **2001**, *113*, 199–213.

(22) Ferrari, S.; Morandi, F.; Motiejunas, D.; Nerini, E.; Henrich, S.; Luciani, R.; Venturelli, A.; Lazzari, S.; Calò, S.; Gupta, S.; Hannaert, V.; Michels, P. A. M.; Wade, R. C.; Costi, M. P. Virtual Screening Identification of Nonfolate Compounds, Including a CNS Drug, as Antiparasitic Agents Inhibiting Pteridine Reductase. *J. Med. Chem.* **2011**, *54*, 211–221.

(23) Cavazzuti, A.; Paglietti, G.; Hunter, W. N.; Gamarro, F.; Piras, S.; Loriga, M.; Allecca, S.; Corona, P.; McLuskey, K.; Tulloch, L.; Gibellini, F.; Ferrari, S.; Costi, M. P. Discovery of Potent Pteridine Reductase Inhibitors to Guide Antiparasite Drug Development. *Proc. Natl. Acad. Sci. U.S.A.* **2008**, *105*, 1448–1453.

- (24) Ferrari, S.; Losasso, V.; Saxena, P.; Costi, M. P. Targeting the Trypanosomatid Enzymes Pteridine Reductase and Dihydrofolate Reductase. *Trypanosomatid Diseases: Molecular Routes to Drug Discovery*; Wiley-Blackwell, 2013; pp 445–472.
- (25) Costi, M. P.; Ferrari, S.; Guerrieri, D.; Henrich, S.; Lazzari, S.; Luciani, R.; Motiejunas, D.; Nerini, E.; Venturelli, A.; Wade, R. C. Uso Di Inibitori Della Pteridina Reduttasi per La Prevenzione E/o Il Trattamento Di Infezioni Parassitarie. ITMI20102191 A1, 2012.
- (26) Corona, P.; Gibellini, F.; Cavalli, A.; Saxena, P.; Carta, A.; Loriga, M.; Luciani, R.; Paglietti, G.; Guerrieri, D.; Nerini, E.; Gupta, S.; Hannaert, V.; Michels, P. A. M.; Ferrari, S.; Costi, P. M. Structure-Based Selectivity Optimization of Piperidine–Pteridine Derivatives as Potent Leishmania Pteridine Reductase Inhibitors. *J. Med. Chem.* **2012**, *55*, 8318–8329.
- (27) Dawson, A.; Tulloch, L. B.; Barrack, K. L.; Hunter, W. N. High-Resolution Structures of Trypanosoma Brucei Pteridine Reductase Ligand Complexes Inform on the Placement of New Molecular Entities in the Active Site of a Potential Drug Target. *Acta Crystallogr., Sect. D: Biol. Crystallogr.* **2010**, *66*, 1334–1340.
- (28) Barrack, K. L.; Tulloch, L. B.; Burke, L.-A.; Fyfe, P. K.; Hunter, W. N. Structure of Recombinant Leishmania Donovanii Pteridine Reductase Reveals a Disordered Active Site. *Acta Crystallogr., Sect. F: Struct. Biol. Cryst. Commun.* **2011**, *67*, 33–37.
- (29) Hu, Y.; Li, C.-Y.; Wang, X.-M.; Yang, Y.-H.; Zhu, H.-L. 1,3,4-Thiadiazole: Synthesis, Reactions, and Applications in Medicinal, Agricultural, and Materials Chemistry. *Chem. Rev.* **2014**, *114*, 5572–5610.
- (30) Upadhyay, S.; Chandra, A.; Singh, R. M. A One Pot Method of Conversion of Aldehydes into Nitriles Using Iodine in Ammonia Water: Synthesis of 2-Chloro-3-Cyanoquinolines. *Indian J. Chem., Sect. B: Org. Chem. Incl. Med. Chem.* **2009**, *48*, 152–154.
- (31) Miyaura, N.; Suzuki, A. Palladium-Catalyzed Cross-Coupling Reactions of Organoboron Compounds. *Chem. Rev.* **1995**, *95*, 2457–2483.
- (32) Borsari, C.; Luciani, R.; Pozzi, C.; Poehner, I.; Henrich, S.; Trande, M.; Cordeiro-Da-silva, A.; Santarem, N.; Baptista, C.; Tait, A.; Di Pisa, F.; Dello Iacono, L.; Landi, G.; Gul, S.; Wolf, M.; Kuzikov, M.; Ellinger, B.; Reinshagen, J.; Witt, G.; Gribbon, P.; Kohler, M.; Keminer, O.; Behrens, B.; Costantino, L.; Nevado, P. T.; Bifeld, E.; Eick, J.; Clos, J.; Torrado, J.; Jiménez-Antón, M. D.; Corral, M. J.; Alunda, J. M.; Pellati, F.; Wade, R. C.; Ferrari, S.; Mangani, S.; Costi, M. P. Profiling of Flavonol Derivatives for the Development of Antitrypanosomatid Drugs. *J. Med. Chem.* **2016**, *59*, 7598–7616.
- (33) Goodey, N. M.; Herbert, K. G.; Hall, S. M.; Bagley, K. C. Prediction of Residues Involved in Inhibitor Specificity in the Dihydrofolate Reductase Family. *Biochim. Biophys. Acta, Proteins Proteomics* **2011**, *1814*, 1870–1879.
- (34) Shanks, E. J.; Ong, H. B.; Robinson, D. A.; Thompson, S.; Sienkiewicz, N.; Fairlamb, A. H.; Frearson, J. A. Development and Validation of a Cytochrome c-Coupled Assay for Pteridine Reductase 1 and Dihydrofolate Reductase. *Anal. Biochem.* **2010**, *396*, 194–203.
- (35) Gibson, M. W.; Dewar, S.; Ong, H. B.; Sienkiewicz, N.; Fairlamb, A. H. Trypanosoma Brucei DHFR-TS Revisited: Characterisation of a Bifunctional and Highly Unstable Recombinant Dihydrofolate Reductase-Thymidylate Synthase. *PLoS Neglected Trop. Dis.* **2016**, *10*, No. e0004714.
- (36) Dewar, S.; Sienkiewicz, N.; Ong, H. B.; Wall, R. J.; Horn, D.; Fairlamb, A. H. The Role of Folate Transport in Antifolate Drug Action in Trypanosoma Brucei. *J. Biol. Chem.* **2016**, *291*, 24768–24778.
- (37) Sienkiewicz, N.; Jaroslowski, S.; Wyllie, S.; Fairlamb, A. H. Chemical and Genetic Validation of Dihydrofolate Reductase-Thymidylate Synthase as a Drug Target in African Trypanosomes. *Mol. Microbiol.* **2008**, *69*, 520–533.
- (38) Deeming, G. M. J.; Collingwood, J.; Pemberton, M. N. Methotrexate and Oral Ulceration. *Br. Dent. J.* **2005**, *198*, 83–85.
- (39) Whittle, S. L.; Hughes, R. A. Folate Supplementation and Methotrexate Treatment in Rheumatoid Arthritis: A Review. *Rheumatology* **2004**, *43*, 267–271.
- (40) Baran, W.; Batycka-Baran, A.; Zychowska, M.; Bieniek, A.; Szepietowski, J. C. Folate Supplementation Reduces the Side Effects of Methotrexate Therapy for Psoriasis. *Expert Opin. Drug Saf.* **2014**, *13*, 1015–1021.
- (41) Leslie, A. G. W. The Integration of Macromolecular Diffraction Data. *Acta Crystallogr., Sect. D: Biol. Crystallogr.* **2006**, *62*, 48–57.
- (42) Kabsch, W. XDS. *Acta Crystallogr., Sect. D: Biol. Crystallogr.* **2010**, *66*, 125–132.
- (43) Evans, P. Scaling and Assessment of Data Quality. *Acta Crystallogr., Sect. D: Biol. Crystallogr.* **2006**, *62*, 72–82.
- (44) Winn, M. D.; Ballard, C. C.; Cowtan, K. D.; Dodson, E. J.; Emsley, P.; Evans, P. R.; Keegan, R. M.; Krissinel, E. B.; Leslie, A. G. W.; McCoy, A.; McNicholas, S. J.; Murshudov, G. N.; Pannu, N. S.; Potterton, E. A.; Powell, H. R.; Read, R. J.; Vagin, A.; Wilson, K. S. Overview of the CCP4 Suite and Current Developments. *Acta Crystallogr., Sect. D: Biol. Crystallogr.* **2011**, *67*, 235–242.
- (45) Vagin, A.; Teplyakov, A. MOLREP: An Automated Program for Molecular Replacement. *J. Appl. Crystallogr.* **1997**, *30*, 1022–1025.
- (46) Murshudov, G. N.; Vagin, A. A.; Dodson, E. J. Refinement of Macromolecular Structures by the Maximum-Likelihood Method. *Acta Crystallogr., Sect. D: Biol. Crystallogr.* **1997**, *53*, 240–255.
- (47) Emsley, P.; Cowtan, K. Coot: Model-Building Tools for Molecular Graphics. *Acta Crystallogr., Sect. D: Biol. Crystallogr.* **2004**, *60*, 2126–2132.
- (48) McNicholas, S.; Potterton, E.; Wilson, K. S.; Noble, M. E. M. Presenting Your Structures: The CCP4mg Molecular-Graphics Software. *Acta Crystallogr., Sect. D: Biol. Crystallogr.* **2011**, *67*, 386–394.
- (49) *Maestro*, Schrödinger Release 2015-4: Version 10.4; Schrödinger, LLC: New York, NY, 2015.
- (50) *LigPrep*, Schrödinger Release 2015-4: Version 3.6; Schrödinger, LLC: New York, NY, 2015.
- (51) Sanschagrin, P. C.; Kuhn, L. A. Cluster Analysis of Consensus Water Sites in Thrombin and Trypsin Shows Conservation between Serine Proteases and Contributions to Ligand Specificity. *Protein Sci.* **1998**, *7*, 2054–2064.
- (52) *SiteMap*, Schrödinger Release 2015-4: Version 3.4; Schrödinger, LLC: New York, NY, 2015.
- (53) Li, H.; Robertson, A. D.; Jensen, J. H. Very Fast Empirical Prediction and Rationalization of Protein pK<sub>a</sub> Values. *Proteins: Struct., Funct., Genet.* **2005**, *61*, 704–721.
- (54) *Glide*, Schrödinger Suite 2015-4: Version 6.9; Schrödinger, LLC: New York, NY, 2015.
- (55) *Jaguar*, Schrödinger Release 2015-4: Version 9.0; Schrödinger, LLC: New York, NY, 2015.
- (56) *QSite*, Schrödinger Release 2015-4: Version 6.9; Schrödinger, LLC: New York, NY, 2015.
- (57) Faria, J.; Moraes, C. B.; Song, R.; Pascoalino, B. S.; Lee, N.; Siqueira-Neto, J. L.; Cruz, D. J. M.; Parkinson, T.; Ioset, J.-R.; Cordeiro-da-Silva, A.; Freitas-Junior, L. H. Drug Discovery for Human African Trypanosomiasis: Identification of Novel Scaffolds by the Newly Developed HTS SYBR Green Assay for Trypanosoma Brucei. *J. Biomol. Screening* **2015**, *20*, 70–81.
- (58) Baker, N.; Glover, L.; Munday, J. C.; Andrés, D. A.; Barrett, M. P.; de Koning, H. P.; Horn, D. Aquaglyceroporin 2 Controls Susceptibility to Melarsoprol and Pentamidine in African Trypanosomes. *Proc. Natl. Acad. Sci. U.S.A.* **2012**, *109*, 10996–11001.
- (59) Chou, T.-C. Theoretical Basis, Experimental Design, and Computerized Simulation of Synergism and Antagonism in Drug Combination Studies. *Pharmacol. Rev.* **2006**, *58*, 621–681.